

Linköping studies in science and technology
Dissertation No. 1087

Multifunctional nanostructured Ti-Si-C thin films

Per Eklund



Linköping University
INSTITUTE OF TECHNOLOGY

Thin Film Physics Division
Department of Physics, Chemistry, and Biology (IFM)
Linköping University
Linköping, Sweden

© **Per Eklund 2007**

Some of the figures in this Thesis appear courtesy of or adapted from originals by
Jens Emmerlich, Manfred Beckers, Jenny Frodelius, and Lars Hultman

Thank you all!

ISBN: 978-91-85715-31-2

ISSN: 0345-7524

Printed by UniTryck, Linköping 2007

Abstract

In this Thesis, I have investigated multifunctional nanostructured Ti-Si-C thin films synthesized by magnetron sputtering in the substrate-temperature range from room temperature to 900 °C. The studies cover high-temperature growth of Ti_3SiC_2 and Ti_4SiC_3 , low-temperature growth of Ti-Si-C nanocomposites, and Ti-Si-C-based multilayers, as well as their electrical, mechanical, and thermal-stability properties. Ti_3SiC_2 and Ti_4SiC_3 were synthesized homoepitaxially onto bulk Ti_3SiC_2 from individual sputtering targets and heteroepitaxially onto $\text{Al}_2\text{O}_3(0001)$ substrates from a Ti_3SiC_2 target at substrate temperatures of 700 – 900 °C. In the latter case, the film composition exhibits excess C compared to the nominal target composition due to differences between species in angular and energy distribution and gas-phase scattering processes. Ti buffering is shown to compensate for this excess C. The electrical-resistivity values of Ti_3SiC_2 and Ti_4SiC_3 thin films were measured to 21-32 $\mu\Omega\text{cm}$ and $\sim 50 \mu\Omega\text{cm}$, respectively. The good conductivity is because the presence of Si layers enhances the relative strength of the metallic Ti-Ti bonds. The higher density of Si layers in Ti_3SiC_2 than in Ti_4SiC_3 explains why Ti_3SiC_2 is the better conductor of the two. Ti_3SiC_2 thin films are shown to be thermally stable up to 1000 – 1100 °C. Annealing at higher temperature results in decomposition of Ti_3SiC_2 by Si out-diffusion to the surface with subsequent evaporation. Above 1200 °C, TiC_x layers recrystallized. Nanocomposites comprising nanocrystalline (nc-)TiC in an amorphous (a-)SiC matrix phase were deposited at substrate temperatures in the range 100 – 300 °C. These nc-TiC/a-SiC films exhibit low contact resistance in electrical contacts and a ductile deformation behavior due to rotation and gliding of nc-TiC grains in the matrix. The ductile mechanical properties of nc-TiC/a-SiC are actually more similar to those of Ti_3SiC_2 , which is very ductile due to kinking and delamination, than to those of the brittle TiC. Epitaxial TiC/SiC multilayers deposited at ~ 550 °C were shown to contain cubic SiC layers up to a thickness of ~ 2 nm. Thicker SiC layers gives a-SiC due to the corresponding increase in interfacial strain energy leading to loss of coherent-layer growth. Nanoindentation of epitaxial $\text{Ti}_3\text{SiC}_2/\text{TiC}_{0.67}$ nanolaminates showed inhibition of kink-band formation in Ti_3SiC_2 , as the lamination with the less ductile TiC effectively hindered this mechanism.

Preface

This Thesis is the result of my PhD studies from 2003 to 2007 with the Thin Film Physics Division of the Department of Physics, Chemistry, and Biology (IFM) at Linköping University. During this time, I have closely collaborated with the Department of Materials Chemistry at Uppsala University, ABB Corporate Research, Impact Coatings AB, and Kanthal AB. My work has been financially supported by the Swedish Agency for Innovation Systems (VINNOVA), the Swedish Research Council (VR) and the Swedish Foundation for Strategic Research (SSF).

Den här doktorsavhandlingen är resultatet av mina doktorandstudier från 2003 till 2007 vid Avdelningen för tunnfilmfysik vid Institutionen för fysik, kemi och biologi (IFM) vid Linköpings universitet. Under den här tiden har jag samarbetat nära med Institutionen för Materialkemi vid Uppsala universitet, ABB Corporate Research, Impact Coatings AB och Kanthal AB. Forskningsanslag från Verket för innovationssystem (VINNOVA), Vetenskapsrådet (VR) och Stiftelsen för strategisk forskning (SSF) har finansierat arbetet.

En populärvetenskaplig svensk sammanfattning finns på sidorna 17-18.

Included papers

MAX-phase thin film growth

Paper I

Homoepitaxy of Ti-Si-C MAX-phase thin films on bulk Ti_3SiC_2 substrates

P. Eklund, A. Murugaiah, J. Emmerlich, Zs. Czigány, J. Frodelius, M. W. Barsoum, H. Högberg, L. Hultman

Accepted for publication in *Journal of Crystal Growth*

Paper II

Magnetron sputtering of Ti_3SiC_2 thin films from a compound target

P. Eklund, M. Beckers, J. Frodelius, H. Högberg, L. Hultman

Manuscript in final preparation

Low-temperature deposition and properties of Ti-Si-C nanocomposite thin films

Paper III

Structural, electrical, and mechanical properties of nc-TiC/a-SiC nanocomposite thin films

P. Eklund, J. Emmerlich, H. Högberg, O. Wilhelmsson, P. Isberg, J. Birch, P. O. Å. Persson, U. Jansson, L. Hultman

Journal of Vacuum Science and Technology B **23**, 2486-2495 (2005)

Paper IV

Microstructure and electrical properties of Ti-Si-C-Ag nanocomposite thin films

P. Eklund, T. Joelsson, H. Ljungcrantz, O. Wilhelmsson, Zs. Czigány, H. Högberg, L. Hultman

Surface and Coatings Technology **201**, 6465-6469 (2007)

Paper V

High-power impulse magnetron sputtering of Ti-Si-C thin films from a Ti_3SiC_2 compound target

J. Alami, **P. Eklund**, J. Emmerlich, O. Wilhelmsson, U. Jansson, H. Högberg, L. Hultman, U. Helmersson

Thin Solid Films **515**, 1731-1736 (2006)

Properties of MAX phases

Paper VI

Electrical resistivity of $Ti_{n+1}AC_n$ ($A = Si, Ge, Sn$; $n = 1 - 3$) thin films

J. Emmerlich, **P. Eklund**, D. Rittrich, H. Högberg, L. Hultman

Submitted for publication

Paper VII

Photoemission studies of Ti_3SiC_2 and nanocrystalline-TiC/amorphous-SiC nanocomposite thin films

P. Eklund, C. Virojanadara, J. Emmerlich, L. I. Johansson, H. Högberg, L. Hultman

Physical Review B **74**, 045417-1-7 (2006)

Paper VIII

Thermal stability of Ti_3SiC_2 thin films

J. Emmerlich, D. Music, **P. Eklund**, O. Wilhelmsson, U. Jansson, J. M. Schneider,

H. Högberg, L. Hultman

Acta Materialia **55**, 1479-1488 (2007)

Carbide multilayers

Paper IX

Epitaxial TiC/SiC multilayers

P. Eklund, H. Högberg, L. Hultman

Submitted for publication

Paper X

Intrusion-type deformation in epitaxial Ti_3SiC_2/TiC_x nanolaminates

O. Wilhelmsson, **P. Eklund**, F. Giuliani, H. Högberg, L. Hultman, U. Jansson

Manuscript in final preparation

My contribution to the included papers

Paper I

I was involved in the planning, performed a large part of the characterization and analysis, and wrote the paper.

Paper II

I was responsible for the planning, performed a large part of the synthesis, characterization and analysis, and wrote the paper.

Paper III

I carried out a major part of the planning, synthesis, characterization, and analysis, and wrote the paper.

Paper IV

I was involved in the planning, performed a large part of the characterization and analysis, and wrote the paper.

Paper V

I was involved in the planning, performed some of the characterization and a large part of the analysis, and wrote parts of the paper.

Paper VI

I was involved in the planning, performed some of the analysis, and contributed extensively to the writing.

Paper VII

I was responsible for planning, analysis, and interpretation of the results, and wrote the paper. (All photoemission measurements were performed by C. Virojanadara and L. I. Johansson.)

Paper VIII

I was involved in the planning and contributed to analysis and writing.

Paper IX

I was responsible for the planning and analysis, performed all synthesis and characterization, and wrote the paper.

Paper X

I was involved in the planning, performed some of the synthesis, characterization, and analysis, and contributed to the writing.

Related publications not included in the Thesis

Ta₄AlC₃: Phase determination, polymorphism, and deformation

P. Eklund, J.-P. Palmquist, J. Höwing, D. H. Trinh, T. El-Raghy, H. Högberg, L. Hultman

Submitted for publication

Weak electronic anisotropy in the layered nanolaminates Ti₃SiC₂, Ti₃GeC₂, and Ti₂GeC

T. H. Scabarozzi, **P. Eklund**, J. Emmerlich, H. Högberg, T. Meehan, J. D. Hettinger, S. E. Lofland, P. Finkel, L. Hultman, M. W. Barsoum

Submitted for publication

Micro- and macroscale tribological behavior of epitaxial Ti₃SiC₂ thin films

J. Emmerlich, G. Gassner, **P. Eklund**, H. Högberg, L. Hultman

Submitted for publication

Phase tailoring of Ta thin films by highly ionized pulsed magnetron sputtering

J. Alami, **P. Eklund**, J.M. Andersson, M. Lattemann, E. Wallin, J. Böhlmark, P. Persson, U. Helmersson

Thin Solid Films **515**, 3434-3438 (2007)

Annealing studies of nanocomposite Ti-Si-C thin films with respect to phase stability and tribological performance

M. Rester, J. Neidhardt, **P. Eklund**, J. Emmerlich, H. Ljungcrantz, L. Hultman, C. Mitterer

Materials Science and Engineering A **429**, 90-95 (2006)

Deposition of ternary thin films within the Ti-Al-C System by dc magnetron sputtering

O. Wilhelmsson, J.-P. Palmquist, E. Lewin, J. Emmerlich, P. O. Å. Persson, H. Högberg, **P. Eklund**, S. Li, R. Ahuja, O. Eriksson, L. Hultman, U. Jansson

Journal of Crystal Growth **291**, 290-300 (2006)

Epitaxial Ti₂GeC, Ti₃GeC₂, and Ti₄GeC₃ MAX-phase thin films grown by magnetron sputtering

H. Högberg, **P. Eklund**, J. Emmerlich, J. Birch, L. Hultman

Journal of Materials Research **20**, 779-782 (2005)

Growth and characterization of MAX-phase thin films

H. Högberg, L. Hultman, J. Emmerlich, T. Joelsson, **P. Eklund**,
J. M. Molina-Aldareguia, J. -P. Palmquist, O. Wilhelmsson, U. Jansson
Surface and Coatings Technology **193**, 6-10 (2005)

Electronic structure investigation of Ti_3AlC_2 , Ti_3SiC_2 , and Ti_3GeC_2 by soft X-ray emission spectroscopy

M. Magnuson, J. -P. Palmquist, M. Mattesini, S. Li, R. Ahuja, O. Eriksson,
J. Emmerlich, O. Wilhelmsson, **P. Eklund**, H. Högberg, L. Hultman, U. Jansson
Physical Review B **72**, 245101-1-9 (2005)

Novel ceramic Ti-Si-C nanocomposite coatings for electrical contact applications

P. Eklund

Winner of the Best Paper Award – 5000 USD

Bodycote Prize Paper Competition 2006

Surface Engineering (in press, 2007)

Comment on "Pulsed laser deposition and properties of $M_{n+1}AX_n$ phase formulated Ti_3SiC_2 thin films"

P. Eklund, J. -P. Palmquist, O. Wilhelmsson, U. Jansson, J. Emmerlich, H. Högberg,
L. Hultman

Tribology Letters **17**, 977-978 (2004)

Synthesis and characterization of Ti-Si-C compounds for electrical contact applications

P. Eklund, J. Emmerlich, H. Högberg, P. O. Å. Persson, L. Hultman,
O. Wilhelmsson, U. Jansson, P. Isberg

Proceedings of the 51st IEEE Holm Conference on Electrical Contacts
Chicago, USA, 26-28 September 2005, p. 277-283

Growth and property characterization of epitaxial MAX-phase thin films from the $Ti_{n+1}(Si, Ge, Sn)C_n$ systems

H. Högberg, J. Emmerlich, **P. Eklund**, O. Wilhelmsson, J.-P. Palmquist, U. Jansson,
L. Hultman

Proceedings of the 11th International Ceramics Congress

Acireale, Sicily, Italy, 4-9 June 2006

Advances in Science and Technology **45**, 2648-2655 (2006)

Patent

Coatings of $M_{n+1}AX_n$ material for electrical contact elements

P. Isberg, P. Eklund, J. Emmerlich, L. Hultman, H. Högberg, H. Ljungcrantz
International Patent no. WO 2005/038985 A3 (Oct 18, 2004)

Acknowledgments

I am grateful to a large number of people who have supported me and/or contributed during the course of this work. In particular, I acknowledge:

- **Lars Hultman**, my supervisor, who “fosters my scientific mind” and always finds the time to constructively criticize and improve my work despite being a very busy person.
- **Hans Högberg**, my co-supervisor and office neighbor, who has supported and helped me in more ways than I can mention, and who never ceases to amaze me with his stories on much tougher life was when *he* was a PhD student.
- **Henrik Ljungerantz**, at Impact Coatings AB, for bringing industrial relevance to (and making money from) this work.
- **Peter Isberg** and **Åke Öberg**, at ABB, for being full of ideas and, despite being in industry, never forgetting the importance of basic research.
- **Torbjörn Selinder**, my mentor at Sandvik Tooling AB, for his encouragement and our discussions on the broader picture of my work and career.
- **Germany**, for teaching us how to play World Cup football, and for such great coworkers as **Jens Emmerlich**, **Jörg Neidhardt**, **Manfred Beckers**...and the list could go on forever.
- **Inger**, **Kalle**, and **Thomas**, the Thin Film Group’s equivalent of “The Force” in Star Wars – the universe would fall apart without them...
- **All other members, past and present, of the Thin Film Physics and Plasma & Coating Physics Divisions**, but especially **Jenny Frodelius**, my ambitious disciple and successor, **Axel Flink**, who I have known since long before we started our PhDs here, **Finn Giuliani**, for his relentless teaching efforts on the finer nuances of cricket and the Queen’s English, **Jones Alami**, for our nice trip to Venice which resulted in extensive scientific collaboration, **Johan Böhlmark**, for tipping me off about this PhD student position in the first place, and **Jens Birch**, the fundamental source of all human knowledge.
- **Friends and collaborators in Uppsala**, i.e., **Jens-Petter Palmquist** (now at Kanthal AB), **Erik Lewin**, **Ulf Jansson**, and especially **Ola Wilhelmsson**, for all the hard work and long lab hours together and apart – we really deserved that seafood buffet in Cocoa Beach!
- **Friends and collaborators in the United States**, i.e., **Rick Haasch**, **Javier Bareno**, and **Ivan Petrov**, University of Illinois at Urbana-Champaign, **Michel Barsoum** and **Sandip Basu**, Drexel University, **Sam Lofland** and **Jeff Hettinger**, Rowan University, for their warm welcomes during my visits, and especially **Ted Scabarozi**, not only for his scientific collaboration but also for his detailed tour of the Wachovia Center and his enlightened information and opinions on the qualities (or lack thereof) of the Philadelphia Flyers.
- **All members of Linköping Judo**, but especially head *sensei* **Lasse Karlsson**, **Leif Kanebrant**, and **Sten Sunnergren**. You are great examples of *jita kyoei*.
- **My parents**, last but certainly not least. Good luck with the new apartment.
- _____ (**your name**), for reading my thesis. (Because you didn’t just read the acknowledgments to check if your name was there, right?)

Table of Contents

PREFACE	5
ACKNOWLEDGMENTS	13
POPULÄRVETENSKAPLIG SAMMANFATTNING PÅ SVENSKA	17
1 INTRODUCTION	19
1.1 A BRIEF HISTORY OF MATERIALS SCIENCE AND ENGINEERING	19
1.2 A BRIEF HISTORY OF THIN FILM TECHNOLOGY	20
1.3 BACKGROUND TO THIS THESIS	20
1.4 OBJECTIVE	21
1.5 OUTLINE	21
2 NANOTECHNOLOGY AND NANOSTRUCTURED MATERIALS	23
2.1 NANOTECHNOLOGY	23
2.2 NANOSTRUCTURED MATERIALS	24
2.2.1 <i>Definitions</i>	24
2.2.2 <i>Nanostructured ternary materials</i>	25
2.2.3 <i>Mechanical properties</i>	25
2.2.4 <i>Electrical properties</i>	26
3 TI-SI-C AND RELATED MATERIALS SYSTEMS	29
3.1 PHASE DIAGRAM	29
3.2 TiC.....	30
3.3 Ti ₅ SiC ₂ AND OTHER MAX-PHASES.....	32
3.4 Ti ₅ Si ₃ C _x AND OTHER NOWOTNY PHASES	35
3.5 LITERATURE REVIEW	35
3.5.1 <i>Chemical Vapor Deposition (CVD)</i>	35
3.5.2 <i>Sputtering</i>	35
3.5.3 <i>Cathodic arc deposition</i>	37
3.5.4 <i>Pulsed laser deposition (PLD)</i>	37
4 THIN-FILM SYNTHESIS	41
4.1 PHYSICAL VAPOR DEPOSITION (PVD)	41
4.1.1 <i>Sputtering</i>	41
4.1.2 <i>Cathodic arc deposition</i>	42
4.1.3 <i>Pulsed laser deposition (PLD)</i>	43
4.2 CHEMICAL VAPOR DEPOSITION (CVD).....	43
5 SPUTTERING	45
5.1 THE PHYSICS OF SPUTTERING	45
5.1.1 <i>What is a plasma?</i>	45
5.1.2 <i>The plasma, floating, and bias potentials</i>	46
5.1.3 <i>The sputtering yield</i>	46
5.1.4 <i>Transport of sputtered species</i>	47
5.1.5 <i>Effects at the substrate</i>	48
5.2 MAGNETRON SPUTTERING.....	49
5.2.1 <i>dc magnetron sputtering</i>	49
5.2.2 <i>High-power impulse magnetron sputtering (HIPIMS)</i>	50

6	THIN-FILM GROWTH.....	53
6.1	NUCLEATION AND GROWTH	53
6.2	EPITAXIAL FILM GROWTH.....	54
6.3	POLYCRYSTALLINE FILM GROWTH	54
6.4	CONTROL OF FILM GROWTH	55
7	CHARACTERIZATION OF MATERIALS.....	59
7.1	STRUCTURAL CHARACTERIZATION.....	59
7.1.1	Scanning Electron Microscopy (SEM).....	59
7.1.2	Transmission Electron Microscopy (TEM).....	59
7.1.3	X-ray Diffraction (XRD).....	60
7.1.4	Atomic Force Microscopy (AFM).....	60
7.2	COMPOSITIONAL CHARACTERIZATION	61
7.2.1	X-ray Photoelectron Spectroscopy (XPS).....	61
7.2.2	Energy-dispersive X-ray Spectroscopy (EDX or EDS).....	62
7.2.3	Ion-beam analysis.....	63
7.3	ELECTRICAL CHARACTERIZATION.....	64
7.3.1	Resistivity.....	64
7.3.2	Electrical contacts	65
7.4	MECHANICAL CHARACTERIZATION	66
7.4.1	Nanoindentation	66
8	SUMMARY AND CONTRIBUTION TO THE FIELD.....	69
8.1	MAX-PHASE THIN-FILM GROWTH	69
8.2	LOW-TEMPERATURE DEPOSITION AND ELECTRICAL PROPERTIES OF Ti-Si-C-BASED NANOCOMPOSITE THIN FILMS	70
8.3	COMPOUND-TARGET SPUTTERING PROCESSES.....	71
8.4	PROPERTIES OF MAX PHASES AND NANOCOMPOSITES.....	72
8.4.1	Electrical properties of MAX phases.....	72
8.4.2	Mechanical properties of nanocomposites and MAX phases	72
8.4.3	Thermal stability.....	73
8.5	MULTILAYER STRUCTURES	73
8.5.1	Epitaxial TiC/SiC multilayers.....	74
8.5.2	Epitaxial TiC/Ti ₃ SiC ₂ multilayers.....	74
9	ADDITIONAL RESULTS	77
9.1	IN-SITU XPS OF Ti-Si-C THIN FILMS.....	77
9.2	MASS SPECTROMETRY.....	78
10	EPILOGUE	83

Multifunktionella nanostrukturerade tunna filmer av titankiselkarbid

Materialteknik har alltid varit en central del av människans historia, och en förutsättning för utvecklingen av civilisationen. Dess betydelse märks inte minst på hur vi uppkallat historiska perioder efter vilka material som använts: stenåldern, bronsåldern och järnåldern (kiselåldern?). Modern materialvetenskap däremot handlar inte bara om att tillverka och utveckla material, utan även om att förstå sambandet mellan tillverkningsprocessen, materialets struktur och dess egenskaper – samt hur denna förståelse kan användas för att designa material. I min avhandling sammanstrålar tre begrepp inom materialvetenskap, (multi-)funktionalitet, nanoteknik (nanostruktur) och tunna filmer.

Inom materialvetenskap och materialteknik skiljer man på begreppen *strukturmaterial*, som väljs ut för sin förmåga att bära en last (t.ex. byggmaterial) och *funktionella material*, där det intressanta är materialets funktion, t.ex. elektriska, magnetiska, optiska eller vissa mekaniska egenskaper. *Multifunktionella* material är material som är utvalda eller designade för att ha flera funktioner – exempelvis god elektrisk ledningsförmåga, nötningsmotstånd och korrosionsmotstånd.

Nanoteknik handlar om material (strukturer, maskiner, etc...) där åtminstone någon dimension är på nanometerskalan (nanometer = miljarddel meter). Men det räcker inte med att enbart vara liten – nanoteknik betyder att man får nya funktioner tack vare storleken. I samhällsdebatten beskrivs nanoteknik ofta utifrån visioner om möjliga framtida kvantdatorer, molekylfabriker, medicinska "cell-robotar", och så vidare; det finns också negativa visioner som den om självkopierande nanorobotar som tar över världen och utrotar allt liv. Men om man ignorerar dessa långsiktiga och/eller långsökta visioner, så är det viktigt att inse att nanotekniken finns i våra vardagsliv redan idag, och det är framför allt som *materialteknik* som nanotekniken har lämnat snackstadiet och blivit verkstad. Många kommersiella produkter idag innehåller *nanostrukturerade material*, det vill säga material där nya funktioner uppnås genom att designa materialets struktur på nanonivå.

Anledningen att man ofta vill belägga en yta med ett lager av något annat är att ytbeläggningen förändrar – förhoppningsvis till det bättre! – egenskaperna hos det belagda objektet. Det är därför man målar huset eller lackerar köksbordet. Med *tunna filmer* menar man ytbeläggningar tunnare än någon eller några mikrometer (miljondels meter). Antireflexbehandlingen på glasögon och teflonet i stekpannan är några exempel från vardagen.

Processen jag använt kallas *sputtring* (egentligen heter det *katodförstoftning* på svenska, men *ingen* använder det ordet!) och äger rum i en vakuumkammare där trycket kan vara så lågt som en biljondel av atmosfärtrycket. Där placerar man det material man vill göra en tunn film av. Sedan släpper man in en gas, oftast en ädelgas som argon, som får bilda ett *plasma*, det vill säga en gas som mest består av laddade partiklar (joner). Argonjonerna accelereras med hög energi och får bombardera materialet; då slås atomer av ämnet ut och sprids i vakuumkammaren. De får sedan kondensera på den yta man vill belägga och bilda en tunn film. En stor fördel med denna "biljard på atomnivå" är att man har väldigt stora möjligheter att styra *hur* filmen bildas och växer. Med andra ord går det att designa filmens struktur och i förlängningen dess egenskaper.

Det material jag studerat är titankiselkarbid, alltså ett *ternärt* material. Det betyder att det består av tre grundämnen (titan, kisel och kol). – Varför ett så krångligt val? Hade det inte varit mycket enklare att bara använda ett eller två grundämnen? Visst hade det varit enklare, men också tråkigare! Det blir visserligen mer komplicerat av att lägga till fler grundämnen, men *flexibiliteten* och *designmöjligheterna* ökar i motsvarande grad. I titankiselkarbidsystemet kan jag tillverka en rad olika typer nanostrukturerade material, där de viktigaste kanske är Ti_3SiC_2 , vars fascinerande struktur påminner om ett laminatgolv på nanonivå och *nanokompositer*, med små titankarbidkristaller inbakade i amorft material. Båda dessa har unika egenskaper tack vare sin nanostruktur – de är hyfsade elektriska ledare, lagom hårda utan att vara för hårda, inte spröda, korrosionsbeständiga och så vidare.

Kort sagt, de är *multifunktionella nanostrukturerade tunna filmer av titankiselkarbid* !

1 Introduction

“-We are living in a material world“

Madonna, “Material Girl”

1.1 A brief history of materials science and engineering

Materials engineering is an ancient discipline. It dates back more than a million years, when the first humans (*homo habilis*) started shaping stone tools instead of using the stones in the same form they were found. Since then, materials engineering has been an integral, and essential, part of human development. This is in particular pointed out by the way we name periods in human prehistory: Stone Age, Bronze Age, and Iron Age. However, the development was driven by trial-and-error, a method that by necessity requires time. An example is “good iron”, discovered by the Hittites¹ in present-day Turkey around 1300 BC by heating iron with charcoal. While the Hittites certainly possessed a high-level empirical knowledge about iron working, it was not until 3100 years later, in 1774, that someone (Swedish chemist Torbern Bergman²) started to understand *how* the formation of “good iron” depended on the addition of carbon. The Hittites’ “good iron” would today be referred to as low-carbon steel.

The first steps towards in-depth understanding of materials were taken upon developing methods for microanalysis. The first known optical microscope was designed by Zacharias and Hans Janssen in the 1590s.³ Development continued, and particularly the 19th century saw vast improvements in microscope design. This accompanied, and permitted, great advances in materials engineering; notably the birth of the modern steel industry.

In the 20th century, the discovery of X-rays, the invention of the electron microscope, and several other techniques allowed studying the structure of materials from atomic to macroscopic level. This century saw a veritable explosion in materials technology, where polymers like rubber and plastics as well as silicon-based electronic materials deserve particular mention. The 20th century also heralded the advent of true *materials science*, which requires in-depth knowledge and understanding of the relationship between the manufacturing process, the structure of the material, and its properties. These three parts are the legs of the chair upon which modern materials science rests, although in recent years, a fourth leg has become increasingly important: theory and modeling. In principle, modern calculation methods allow new materials to be designed in the computer, and are rapidly developing into invaluable tools in materials science and engineering.

1.2 A brief history of thin film technology

Thin films for decorative purposes have existed since the dawn of civilization. A prime example is the leaf gold (with a thickness down to $0.3\ \mu\text{m}$) of remarkable quality found in ancient Babylonia and Egypt. However, deliberate usage of thin films where the practical functionality rather than the appearance is of importance, is of a younger date. In the early 1800s, electroplating, which was the first widespread thin film deposition technique, was developed. Compared to other methods, electroplating has the advantage of not requiring vacuum. The quality of the vacuum was a limiting factor for many thin film deposition techniques.

The arguably oldest among the methods today referred to as physical vapor deposition (PVD) is the cathodic-arc deposition technique, originally discovered by Joseph Priestley in the mid-1700s. However, at the time, nobody was able to find a practical application and the method remained a partially forgotten curiosity until Thomas Alva Edison revived in the 1880s.⁴ Sputtering was discovered in 1852 by W. R. Grove, who reported on the ejection of atoms from a material in a vacuum resulting from bombardment by positive ions.⁵ At first, the sputtering phenomenon was seen as a nuisance resulting in contamination of vacuum tubes. However, in the late 1800s, it was used to coat mirrors with silver and similar metals. It found commercial use in the early 1900s.⁶

Together with other types of evaporation, these techniques have developed into the backbone of the modern PVD industry, which has applications in such diverse areas as microelectronics, optical coatings, hard coatings on tools, and decorative coatings.

1.3 Background to this thesis

In the 1960s, Jeitschko and Nowotny synthesized many of the materials that are today known as MAX phases, and determined their structure.^{7,8} However, the modern interest arose in the mid-1990s, when Barsoum synthesized comparatively phase-pure samples of the MAX phase Ti_3SiC_2 , and discovered a material with a unique combination of metallic and ceramic properties: it exhibited high electrical and thermal conductivity, and it was machinable.⁹ Still, it was extremely resistant to oxidation and thermal shock. In 2001, Barsoum visited Linköping, and MAX-phase research collaboration was initiated. Simultaneously, there was significant industrial interest, as ABB saw the MAX phases as potential electrical-contact materials. A pre-study by Seppänen¹⁰ showed very promising results. This resulted in several research grants on MAX-phases, including one from the Swedish Agency for Innovation Systems (VINNOVA). This project, *Industrialization of MAX-phase coatings*, was a joint university-industry project with the partners Linköping University, Uppsala University, ABB, Kanthal, and the small Linköping-based company Impact Coatings, a spin-off from the Thin Film Physics Division at the university. Impact Coatings are marketing the MAX coating and the coating process, while Kanthal, in Hallstahammar, are marketing bulk MAX phases. The project also funded a large part of my doctoral studies at Linköping University in close collaboration with the industrial partners.

When it ended in 2005, the project had resulted in a patent,¹¹ and Impact Coatings were listed on the Stockholm stock exchange. The industrialization process has continued within other projects, and was one important reason for why Linköping in 2006

was awarded the major research and industrialization center* on Functional Nanoscale Materials (*FunMat*), jointly funded by VINNOVA, industry, and Linköping University. One reason for this success is a unique, and rapid, way of working together, with fundamental and applied research at the universities in parallel with the product development and industrialization at the companies. This is a quite remarkable contrast to the traditional sequential method, where the basic research is performed first, followed by product development, and only after that, industrialization takes place.

1.4 Objective

The main objective of my thesis work is to understand, on a fundamental level, the physics and materials science of the Ti-Si-C materials system. A secondary objective of the underlying research project (not essential to the Thesis as such) is that this understanding should enable industrialization of Ti-Si-C-based coatings by the company partners. This knowledge transfer goes both ways; continuous feedback on industrial requirements is an inspiration for my research.

1.5 Outline

This Thesis is outlined as follows:

- Chapter 1 gives the background and sets the scope and objective of my thesis.
- Chapter 2 is an introduction to nanotechnology and, in particular, nanostructured materials.
- Chapter 3 is a review of the Ti-Si-C materials system and of previous work on thin film synthesis of these and related materials.
- Chapter 4 is an introduction to sputtering, the synthesis method I have used, as well as other relevant methods.
- Chapter 5 is a more detailed discussion on magnetron sputtering.
- Chapter 6 is an overview of the physics of film growth.
- Chapter 7 is a presentation of the methods I have used for materials analysis.
- Chapter 8 is a summary of the results in the papers included in the thesis, and a discussion on how my Thesis contributes to the research field.
- Chapter 9 contains preliminary results that are directly relevant to the main topic of the Thesis.
- Chapter 10 offers some final perspectives.

* *FunMat* is a “Vinnova Excellence Center in Research and Innovation”.

-
- ¹ A. W. Pense *Iron through the ages* Materials characterization 45 353 (2000)
- ² Nordisk Familjebok Gernandts boktryckeri-aktiebolag, Stockholm 1878. Accessible in digital format at <http://runeberg.org/nf/> (February 19, 2007)
- ³ Molecular expressions Optical microscopy primer <http://micro.magnet.fsu.edu/primer> (February 19, 2007)
- ⁴ A. Anders *Tracking Down the Origin of Arc Plasma Science I. Early Pulsed and Oscillating Discharges* IEEE Transactions on Plasma Science 31 1052 (2003)
- ⁵ W. R. Grove *On the Electro-Chemical Polarity of Gases* Philosophical Transactions of the Royal Society of London 142 87 (1852)
- ⁶ H. F. Fruth *Cathode sputtering, a commercial application* Physics 2 280 (1932)
- ⁷ W. Jeitschko and H. Nowotny *Die Kristallstruktur von Ti_3SiC_2 – ein neuer Komplexcarbid-Typ* Monatshefte für Chemie 98 329 (1967)
- ⁸ H. Nowotny *Strukturchemie einiger verbindungen der übergangsmetalle mit den elementen C, Si, Ge, Sn* Progress in Solid State Chemistry 2 27 (1970)
- ⁹ M. W. Barsoum *The $M_{n+1}AX_n$ -Phases: a new class of solids* Progress in Solid State Chemistry 28 201 (2000)
- ¹⁰ T. Seppänen, J.-P. Palmquist, P.O.Å. Persson, J. Emmerlich, J. Molina, J. Birch, U. Jansson, P. Isberg, and L. Hultman *Structural characterization of epitaxial Ti_3SiC_2 thin films* Proceedings of the 53rd Annual Meeting of the Scandinavian Society for Electron Microscopy 142 (2002) (Ed. J. Keränen and K. Sillanpää, Tampere University, Finland, ISSN 1455-4518)
- ¹¹ P. Isberg, P. Eklund, J. Emmerlich, L. Hultman, H. Högberg, and H. Ljungcrantz *Coatings of $M_{n+1}AX_n$ material for electrical contact elements* International Patent WO 2005/038985 A3 (Oct 18, 2004)

2 Nanotechnology and nanostructured materials

“-Skate to where the puck is going, not to where it’s been.”

Wayne Gretzky

This chapter is a brief introduction to the vast field of *nanotechnology*. Further, it introduces the concepts of *multifunctional* and *nanostructured* materials, and offers some relevant examples.

2.1 Nanotechnology

The prefix *nano* is currently one of the most used – and misused¹ – terms in science and technology. There are “nanotechnology”, “nanomaterials”, “nanoscience”, “nanocrystallites”, and so on. The word refers to the size (*nanos* is Greek for *dwarf*); to be in the “nano realm” a particle (structure, machine, etc...) should be, by convention, smaller than ~100 nm in at least one dimension, although the limit is not strict. However, being small is not enough. Nanotechnology is where *new* (or greatly improved) functionality of materials (structures, machines, etc...) is achieved by nanoscale design, i.e., the properties should *not* be conceivable without working in the nano realm.² This is indeed a revolutionary approach to materials science and technology; traditionally, it is not expected that the properties of materials depend on their size. To exemplify, the conductivity of a piece of copper or the hardness of steel do not depend on the size of the metal pieces.

In the public debate, nanotechnology is often equated with its more visionary concepts.³ Quantum computers, “factories” on the molecular scale, and cellular robots injected into human bodies to detect cancer tumors only a few cells large are examples of such conceivable inventions that would revolutionize society – if they are at all possible to realize. There are also negative visions,³ the most well-known* being the “grey-goo” scenario of self-replicating nanorobots taking over the world and destroying life as we know it.

However, leaving the visions aside, nanotechnology *today* is primarily a *materials* technology – many nanomaterials are available in commercial products.[†] To a large extent, the current emphasis is – and should be – on incorporating nanotechnology as

* And probably the most extreme! The “grey-goo” scenario has had some impact in the public debate after it was popularized by Michael Crichton’s bestselling novel *Prey*. It is not a very good novel, though – if you want to read Crichton, stick to his more realistic work, like *Jurassic Park*.

† Current Swedish examples of such products are Sandvik’s *Nanoflex*, Höganäs’ *Somalloy*, and – of course – Impact Coatings’ *MaxPhase*.

part of both new and existing applications and products, rather than developing a separate “nanotechnology industry”.⁴ As an essential contribution to this development, much current work in both industry and academia is aimed at designing *nanostructured materials*.

2.2 Nanostructured materials

2.2.1 Definitions

The fundamental difference between nanostructured materials and “ordinary” materials originates from the ratio of surface or interface atoms to bulk atoms. This ratio is negligible in ordinary materials, but can be very high in a nanostructured material (the extreme case is that all atoms are surface or interface atoms). This means that in nanostructured materials, surface and interface effects are important or even dominant.

The term *nanocomposite* refers to a designed material consisting of two or more phases, segregated on the nanoscale. It is important to distinguish between *nanocomposite materials* and *nanocrystalline materials*. The latter⁵ refers to any material with crystallites in the nanometer range. It can consist of only one phase. A nanocomposite, on the other hand, should contain at least two phases, and they need not be crystalline. Obviously, a nanocomposite can consist of two nanocrystalline phases,⁶ but “nanocomposite” is a broad concept.

Finally, the term *multifunctional* needs to be defined. In materials science and technology, there is a distinction between *structural* and *functional* materials. According to Cahn:⁷

Structural materials are selected for their load-bearing capacity, functional materials for the nature of their response to electrical, magnetic, optical, or chemical stimuli; sometimes a functional material is even chosen for aesthetic reasons. It is much harder to define a functional material accurately than it is to distinguish a structural material.

As Cahn points out, the definition of a *functional* material is not self-evident. For example, his definition excludes *mechanical* stimuli, which is a much broader term than simply “load-bearing”; low-friction and wear-resistant materials are clearly functional materials. Some materials may fit into both categories, i.e., they are both structural and functional. Furthermore, it can be questioned whether “aesthetic reasons” can be considered a “function” – perhaps *decorative* materials should be a separate category (if so, an important one – especially from a commercial point of view). Ignoring these complications with the definition of *functional*, however, *multifunctional materials* can be defined as functional materials with several (at least two) functions. Finally, it is important to note that the two concepts of “functional” and “structural” materials are general – they are unrelated to “nanostructured” materials. The remaining sections of this chapter will present some relevant examples of materials that are *both* nanostructured and (multi-)functional.

2.2.2 Nanostructured ternary materials

A main theme of my work has been to investigate nanostructured *ternary* thin films. Adding a third element into a binary materials system increases the flexibility in the constituents of the materials system, and consequently offers opportunities for design of new materials, including ternary phases and composites of binary phases. These opportunities are schematically illustrated in Figure 2.1, which shows a phase-composition diagram of a generic ternary system containing the three elements M, A, and X.

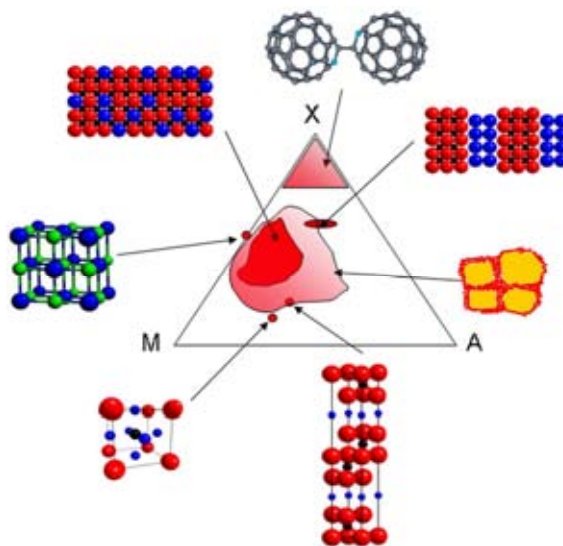


Figure 2.1 Phase-composition diagram of a generic ternary system with the elements M, A, and X.

Although simplified, the generic system illustrated in Figure 2.1 indicates how the nanostructure of materials can be designed by variation of the composition within a ternary system. However, alteration of the nanostructure would be of limited interest if it were not for the fact that it allows tailoring of materials for desired *properties*.

2.2.3 Mechanical properties

One commonly discussed issue in the field of nanocomposite coatings is the search for superhard materials.^{8,9} The ‘intrinsically superhard’ materials, diamond and c-BN (cubic BN), have hardness approaching 100 GPa (‘superhardness’ is conventionally defined as hardness above 40 GPa). In the mid-1990s, a great deal of interest was directed towards the generic nanoscale design concept for superhard coatings proposed by Vepřek and Reiprich.¹⁰ This concept is based on a two-phase nanocomposite, with a nanocrystalline (nc-) phase embedded in an amorphous (a-) matrix; the archetypical example is nc-TiN/a-SiN_x. Vepřek reported extremely high hardness values⁸ for such nanocomposites, well above 50 GPa and in one case even 105 GPa, i.e., a higher value than that of diamond. These exceptionally high values have been questioned;¹¹

nevertheless, the design concept remains relevant. The idea is based on the traditional hardening mechanism of grain-size reduction in single-phase materials (Hall-Petch hardening). A small grain size means that there is a large volume fraction of grain boundaries that hinder dislocation motion, resulting in a higher hardness. Vepřek proposed that a nanocomposite consisting of crystallites a few nanometers large embedded in a monolayer-thick amorphous tissue (or matrix) phase, such as the model system nc-TiN/a-SiN_x, should exhibit very high hardness since the structure itself hinders dislocation motion. While the absolute hardness values may be debated,¹¹ this type of nanostructured material does exhibit high hardness and even superhardness. Recent debate^{12,13} in this field has addressed the nature of the tissue phase,¹⁴ and has indicated that the possibility to have a *crystalline* rather than *amorphous* tissue phase in a nanocomposite must be taken into account. This may provide high interfacial bond strength while retaining the ability to hinder dislocation gliding and grain-boundary sliding. **Paper IX** (see also section 8.5.1) is my contribution to this debate.

Superhard nanocomposites are undeniably nanostructured; however, they are not *per se* multifunctional, as superhardness is just *one* function.[‡] It is, however, clear that superhardness alone is not very useful – it must be combined with other properties, especially toughness (i.e., resistance to fracture and cracking),¹⁵ but often also corrosion-resistance. Thus, in applications such as wear-resistant coatings for cutting tools, there is a need for a multifunctional material; one that is hard, tough, and corrosion-resistant.

2.2.4 Electrical properties

For pure metals, there are two main effects of nanostructure on electrical properties. One is a small grain size (typically < 50 nm), which leads to increased resistivity due to grain-boundary scattering of electrons. The other is increased resistivity due to surface scattering, particularly relevant for thin films. Both these effects arise because of the nanoscale dimensions involved, as the grain size and film thickness are of the same order of magnitude as the mean free path of electrons. There are standard analytical models available; the Fuchs-Sondheimer (FS) model addresses surface scattering, and grain-boundary scattering is accounted for by the Mayadas-Schatzkes (MS) model. The two effects are additive, and can be modeled by adding the FS and MS terms[§] of the resistivity.¹⁶

The combined FS-MS model is applicable for nanocrystalline pure metal films. To model conduction in a nanocomposite is more complicated, but *percolation* models can often be used. For the purpose of electrical properties, a nanocomposite in its simplest form can be modeled as spherical (or ellipsoidal) conducting particles in an insulating matrix. There is then a geometrical percolation threshold, i.e., at some volume fraction of the conducting phase, the spherical particles will connect to form a continuous conducting phase.¹⁷ In the ideal model, the nanocomposite will be an insulator below the percolation threshold, and a conductor above it. This model is applicable to, e.g., noble-metal nanoparticles dispersed in a dielectric matrix such as a polymer.¹⁸ With modifications, percolation models can reasonably account for conduction in some nanocomposites with two conducting phases, or when the matrix is

[‡] If hardness is a function at all – it could easily be argued that superhard coatings should be regarded as *structural* materials. Hardness is, after all, a measure of the load-bearing capacity of a material.

[§] The equations are not very complicated, but I omit them here as they are not central to this work.

the conducting phase.¹⁹ On the other hand, the conduction mechanisms in more complex nanocomposites (such as the Ti-Si-C-Ag thin films in **Paper IV**) are difficult to simulate.

The two previous paragraphs dealt with the effect of nanostructure on resistivity. Again, however, low resistivity is just *one* function. A relevant example of an application area where *multifunctional* materials with low resistivity are needed is electrical contacts (see also section 7.3.2). Many nanocomposites intended for electrical applications are based on noble metals like Ag, Au, or Cu. These are good conductors and they are corrosion-resistant. In many applications, however, their mechanical (and tribological) properties are unsatisfactory. Thus, they can be reinforced by ceramic nanoparticles in order to improve the wear-resistance and hardness, as has been shown for Cu/TiB₂ and Ag/TiC nanocomposites.^{20,21} However, in some cases, a significant increase in the amount of the ceramic constituent may result in a severe decrease in electrical conductivity.²⁰ In the present work, I have approached the problem from the other direction, using a conducting *ceramic* as the starting point to design a multifunctional thin-film material for (but not necessarily exclusively for) electrical-contact applications. **Papers III** and **IV** are dedicated to this topic.

-
- ¹ P. DiJusto *Nanosize Me* Scientific American Dec. 2004 p.12
- ² See, e.g., The US National Nanotechnology Initiative, www.nano.gov (March 7, 2007)
- ³ A- S. Karhi *Den lilla tekniken i det stora skeendet – nanoteknik, gränser och omvärldsuppfattningar* Ph. D. Thesis, Linköping Studies in Arts and Science no. 353, ISBN 91-85523-83-6, Linköping University (2006)
- ⁴ E. Perez and P. Sandgren *Nanoteknikens Innovationssystem* VINNOVA Analys VA 2007:01, ISBN 978-91-85084-71-5 (2007)
- ⁵ S. C. Tjong and H. Chen *Nanocrystalline materials and coatings* Materials Science and Engineering R 45 1 (2004)
- ⁶ U. Herr, J. Jing, U. Gonser, and H. Gleiter *Alloy effects in consolidated binary mixtures of nanometer-sized crystals investigated by Mössbauer spectroscopy* Solid State Communications 76 197 (1990)
- ⁷ R. W. Cahn *The coming of materials science* Pergamon, Amsterdam (2001)
- ⁸ S. Vepřek *The search for novel, superhard materials* Journal of Vacuum Science and Technology A 17(5) 2401 (1999)
- ⁹ S. Vepřek, M. G. J. Vepřek-Heijman, P. Karvankova, and J. Prochazka *Different approaches to superhard coating and nanocomposites* Thin Solid Films 476 1 (2005)
- ¹⁰ S. Vepřek and S. Reiprich *A concept for the design of novel superhard coatings* Thin Solid Films 268 64 (1995)
- ¹¹ J. Musil, H. Zeman, F. Kunc, and J. Věček *Measurement of hardness of superhard films by microindentation* Materials Science and Engineering A 340 281 (2003)
- ¹² H. Söderberg, M. Odén, T. Larsson, L. Hultman, and J. M. Molina-Aldareguia *Epitaxial stabilization of cubic-SiN₄ in TiN/SiN_x multilayers* Applied Physics Letters 88 191902 (2006)
- ¹³ S. Vepřek and M. G. J. Vepřek-Heijman *The formation and role of interfaces in superhard nc-Me_nN/a-Si₃N₄ nanocomposites* Surface and Coatings Technology 201 6064 (2007)
- ¹⁴ L. Hultman, J. Bareño, A. Flink, H. Söderberg, K. Larsson, V. Petrova, M. Odén, J. E. Greene, and I. Petrov *Interface structure in superhard TiN-SiN nanolaminates and nanocomposites: Film growth experiments and ab initio calculations* Physical Review B 75 130711 (2007)
- ¹⁵ S. Zhang, D. Sun, Y. Fu, and H. Du *Toughening of hard nanostructural thin films: a critical review* Surface and Coatings Technology 198 2 (2005)
- ¹⁶ C. Durkan and M. E. Welland *Size effects in the electrical resistivity of polycrystalline nanowires* Physical Review B 61 14215 (2000)
- ¹⁷ E. J. Garbozci, K. A. Snyder, J. F. Douglas, and M. F. Thorpe *Geometrical percolation threshold of overlapping ellipsoids* Physical Review E 52 819 (1995)
- ¹⁸ U. Schürmann, W. Hartung, H. Takele, V. Zaporozhchenko, and F. Faupel *Controlled syntheses of Ag-polytetrafluorethylene nanocomposite thin films by co-sputtering from two magnetron sources* Nanotechnology 16 1078 (2005)
- ¹⁹ K. Sedláčková, P. Lobotka, I. Vávra, and G. Radnóczy *Structural, electrical and magnetic properties of carbon-nickel composite thin films* Carbon 43 2192 (2005)
- ²⁰ J. P. Tu, W. Rong, S. Y. Guo, and Y. Z. Yang *Dry sliding wear behavior of in situ Cu-TiB₂ nanocomposites against medium carbon steel* Wear 255 832 (2003)
- ²¹ J. L. Endrino, J. J. Nainaparampil, and J. E. Krzanowski *Microstructure and vacuum tribology of TiC-Ag composite coatings deposited by magnetron sputtering-pulsed laser deposition* Surface and Coatings Technology 157 95 (2002)

3 Ti-Si-C and related materials systems

“I know many beautiful songs from your home county, Carbon [...] and I hitchhiked through there and stayed in the homes of miners.”

Pete Seeger

This chapter reviews the materials systems Ti-Si-C, starting with a discussion on the phase diagram. It then addresses the binary carbide TiC and its properties, continues with a discussion of the ternary phases in the system, most notably the MAX phases, and ends with a literature review, primarily on the Ti-Si-C system, with emphasis on previous work directly relevant for my Thesis.

3.1 Phase diagram

Any study of a ternary materials system should begin with its phase diagram, and the number one authority on the subject is the *Handbook of ternary alloy phase diagrams*.¹ Numerous authors have reported phase diagrams for the Ti-Si-C system, experimentally and/or theoretically determined, for example Viala *et al.*,² Wakelkamp *et al.*,³ Touanen *et al.*,⁴ and Sambasivan and Petsukey.⁵

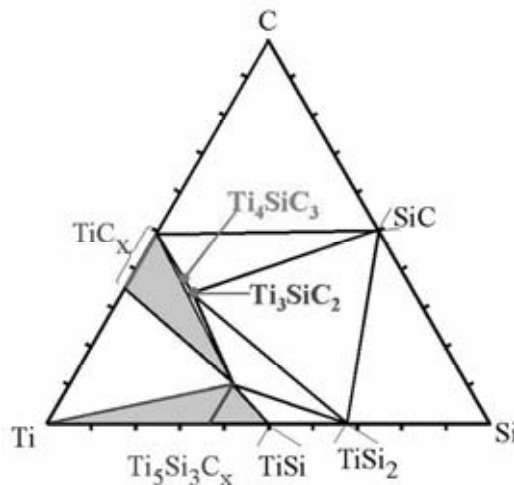


Figure 3.1 Phase diagram of the Ti-Si-C system at 1000 °C, after Viala *et al.*² Also shown is the metastable phase Ti_4SiC_3 (see section 3.3).

A binary phase diagram is usually drawn as a function of composition and temperature. A problem when studying a ternary phase diagram is that it is very difficult to include the temperature as a parameter. Instead, ternary phase diagrams are normally reported as isothermal cross sections. The Ti-Si-C cross sections reported in the literature are typically determined at temperatures of 1000 °C – 1300 °C. Figure 3.1 shows a simplified Ti-Si-C diagram, after Viala *et al.*,² at 1000 °C. The silicides Ti₃Si and Ti₅Si₄ are not stable in the presence of carbon, and therefore not shown.

In the phase diagram in Figure 3.1, it can be seen that there is one stable ternary phase in the Ti-Si-C, the MAX phase Ti₃SiC₂ (see section 3.3). The metastable Ti₄SiC₃ is also shown. Further, the silicide Ti₅Si₃ normally contains dissolved C, and should therefore be written Ti₅Si₃C_x. This is called a Nowotny phase. MAX phases and Nowotny phases will be described in sections 3.3 and 3.4, respectively. The stable binary phases are TiC, SiC, TiSi, and TiSi₂.

A few reservations about the phase diagrams are in order. First, they are all reported at temperatures of 1000 °C – 1300 °C. This is close to the substrate temperature used for synthesis of MAX phases in **Papers I** and **II**, but much higher than the range from room temperature to 300 °C used for low-temperature deposition of Ti-Si-C nanocomposites used in **Paper III** and **IV**. Second, phase diagrams represent the situation at thermodynamic equilibrium. As will be discussed in chapters 4 and 5, magnetron sputtering is a synthesis method operating far from equilibrium. For these reasons, it is necessary to interpret phase diagrams with care.

This chapter continues with a discussion on the most relevant phases in the Ti-Si-C system. Before discussing the ternary phases, it is suitable to review the structure and properties of the binary carbide TiC.

3.2 TiC

TiC is one of the interstitial transition-metal carbides. The crystal structure is a NaCl structure, with two interleaved fcc lattices, one with metal atoms and one with C atoms. In interstitial carbides, the metal atoms form a close-packed structure with the carbon atoms placed in interstitial octahedral sites, as shown in Figure 3.2. In the binary transition-metal carbides, the thus formed octahedra share edges. According to the Hägg rule, interstitial compounds are formed when the ratio between the atomic radii, r_C/r_{metal} , is smaller than 0.59.⁶ This criterion is fulfilled for all group IV-VI transition metals, except Cr. It is important to note here that the interstitial carbides (and nitrides) are something different from interstitial solid solutions of carbon (or nitrogen) in metals. Ti metal is hcp and remains so when carbon dissolves interstitially. When it forms TiC, however, the lattice is fcc. Generally, if the transition metal has a hexagonal structure, the corresponding carbide will be cubic; if the metal is bcc, the carbide can be hexagonal or fcc; while no fcc metals form interstitial carbides. This is because the crystal structure depends not only on the atomic sizes, but also on the stabilizing effect of the interstitial and on metal-metal interaction.

Some of the most notable properties of TiC, as well as the other interstitial carbides are high hardness, high melting point, and low thermal conductivity. While its hardness is high enough to consider it a ceramic, its electronic-transport mechanism is that

of a metal, i.e., electric charge is transported via conduction electrons. The concentration of conduction electrons is, however, low; the density of states at the Fermi level ($DOS(E_f)$) is ~ 0.08 states/(eVcell)⁻¹.⁷ $DOS(E_f)$ is a good theoretical indicator of the conductivity of a material. A high $DOS(E_f)$ means that many electrons are available for conduction, i.e., the material is a good conductor. In comparison, for an insulator, $DOS(E_f)$ is zero, since the Fermi level is inside a bandgap.

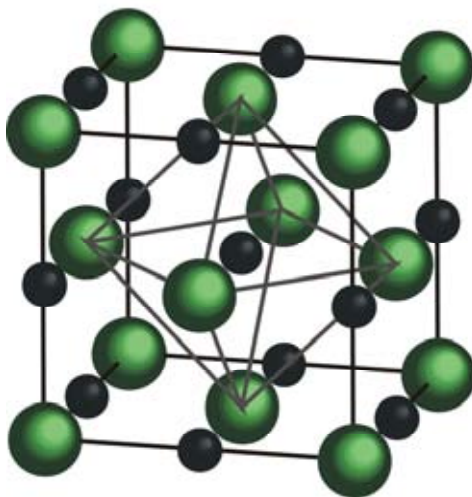


Figure 3.2 The octahedral structural arrangement in the transition-metal carbides, e.g., TiC. Large atoms are Ti.

A further important characteristic of the interstitial carbides is their pronounced non-stoichiometry.⁸ All transition-metal carbides have a significant amount of carbon vacancies and a very large stability range. The carbon-to-metal ratio can assume values in the range of approximately 0.47-0.97 without any structural change.^{9,10} This is usually written TiC_x , where x is the carbon-to-metal ratio. The lattice parameter varies strongly with the stoichiometry, from ~ 4.296 Å at $x = 0.5$ to a maximum of ~ 4.332 Å at $x = 0.85$; note that the maximum value of the lattice parameter is *not* at near-stoichiometric conditions.

The high concentration of carbon vacancies extensively affects the physical properties of TiC_x . For example, the electrical resistivity of bulk TiC_x has been reported to range from 70 ± 10 $\mu\Omega\text{cm}$ at near-stoichiometry to close to 200 $\mu\Omega\text{cm}$ for $TiC_{0.8}$.⁷ This is a consequence of vacancy scattering of the electrons. In the same composition range, the hardness varies by a factor of two because of the strong covalent bonding, which increases with increasing x .⁷

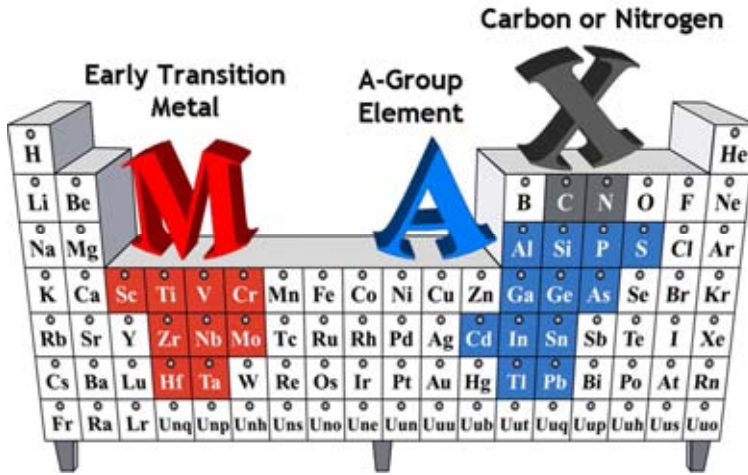


Figure 3.3 Periodic chart illustrating the elements forming MAX phases.

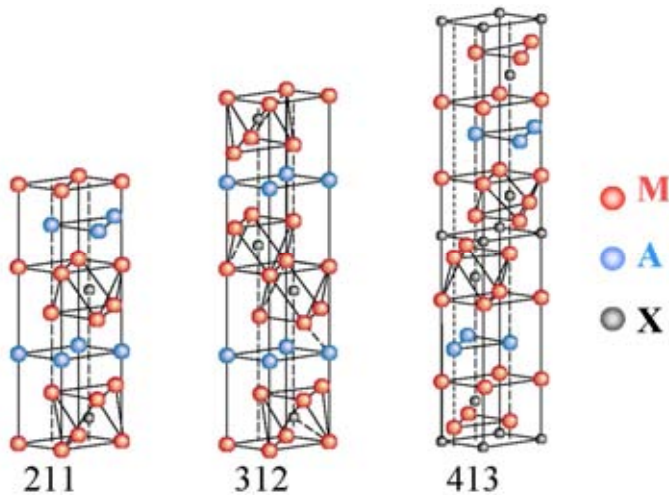


Figure 3.4 Stacking sequences of the 211, 312, and 413, MAX phases.

3.3 Ti_3SiC_2 and other MAX-phases

In the 1960s, Jeitschko and Nowotny^{11,12} synthesized more than 30 ternary carbides and nitrides with similar characteristics and chemical compositions, e.g., Ti_2AlC , Nb_2GaC , and Hf_2InC . With a general formula, they can be described as M_2AX , where

M is a transition metal, A is an A-group element, and X is C and/or N.* These are known as Hägg phases (H phases).^{13,†} Later, related compounds with M_3AX_2 and M_4AX_3 stoichiometry were discovered.¹⁴ This led to the introduction of the nomenclature $M_{n+1}AX_n$ ($n = 1, 2, \text{ or } 3$).¹⁴ The different MAX stoichiometries are often referred to as 211 ($n = 1$), 312 ($n = 2$), and 413 ($n = 3$). The elements forming MAX phases are illustrated in Figure 3.3.

The MAX phases experienced a renaissance in the mid-1990s, when Barsoum synthesized relatively phase-pure samples of the MAX phase Ti_3SiC_2 , and discovered a material with a unique combination of metallic and ceramic properties: it exhibited high electrical and thermal conductivity, and it was machinable. Still, it was extremely resistant to oxidation and thermal shock.¹⁴

In order to understand these remarkable properties, it is necessary to study the crystal structure of the MAX phases. Figure 3.4 shows the hexagonal unit cells of the 211, 312, and 413 MAX phases. They consist of M_6X octahedra, or specifically Ti_6C , interleaved with layers of A elements (e.g., Si or Ge). The number of A-element layers thus inserted decides what MAX polytype is formed (211, 312, or 413). The MAX phases are structurally closely related to their MX counterparts, the M_6X (Ti_6C) edge-sharing octahedral building block is the same as in the binary carbide. There are two different M sites in the MAX structure, those adjacent to A, and those not. In Ti_3SiC_2 , they are referred to as Ti(1) and Ti(2), respectively. There are also two nonequivalent X sites. Note that the MAX structure is *very* anisotropic: Ti_3SiC_2 has the lattice parameters $a = 3.06 \text{ \AA}$ and $c = 17.7 \text{ \AA}$. This has a strong effect on the mechanical and electrical properties of the MAX phases.

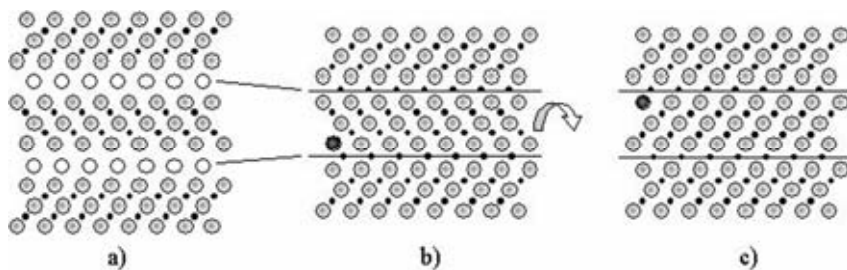


Figure 3.5 Structural relation between TiC and MAX phases: a) The Ti_3C_2 layers are twinned to each other separated by the Si layer acting as a mirror plane. De-twinning to TiC can be observed upon, b) removal of the Si plane and, c) rotation of the Ti_3C_2 layer.

The structural relationship between transition-metal carbides and MAX phases, exemplified by TiC and Ti_3SiC_2 , can further be illustrated by a model proposed by Bar-

* The notation originally used by Nowotny was T-M-X rather than M-A-X. Nowotny's notation was not restricted to $M_{n+1}AX_n$ phases, but also included many other complex ternary carbides and nitrides, e.g., perovskites (T_3MC), and what is today known as Nowotny phases; see section 3.4.

† Named after Gunnar Hägg (1903-1986), professor of general and inorganic chemistry at Uppsala University 1937-1969. Originally,¹³ "Hägg phases" referred to interstitial transition-metal compounds. The meaning has altered with time, and in the MAX-phase literature, "H phase" or "Hägg phase" is synonymous with " M_2AX phase".

soum.¹⁴ This model is shown in Figure 3.5. Here, the TiC layers between Si sheets in Ti₃SiC₂ represent TiC (111) planes. The spacing between adjacent Ti atoms within the TiC layers is the (111) interplanar distance. The Ti₃C₂ layers are twinned to each other separated by the Si layer acting as a mirror plane. In Figure 3.5, de-twinning to TiC can be observed upon removal of the Si plane and rotation of the Ti₃C₂ layer.

While the bulk of this work deals with Ti-Si-C thin films, **Paper VI** investigates the effect of A-element substitution in Ti-A-C MAX phases on electrical properties. **Paper VI** concentrates on the elements in the same column as Si in the periodic chart, i.e., Ge and Sn. As a background, Table 3-1 lists literature values of electrical and mechanical properties of Ti₃SiC₂, Ti₃GeC₂, and TiC_x. Notably, the electrical resistivity is an order of magnitude lower in the MAX phases than in TiC_x. This is consistent with what is expected from theoretical calculations with density functional theory (DFT), which result in $DOS(E_f)$ values of 4.38 states/(eVcell)⁻¹ (for Ti₃SiC₂) or 4.65 states/(eVcell)⁻¹ (for Ti₃GeC₂), compared to 0.08 states/(eVcell)⁻¹ for TiC.¹⁵ The difference in conductivity can be attributed to the presence of Si or Ge, which weakens the Ti(1)-C bonds and thus enhances the relative strength of the metallic Ti(1)-Ti(1) bonds within the basal planes. Consequently, a material with a stronger metallic character and hence higher conductivity than TiC is obtained. It is worth noting that DFT calculations¹⁵ yield a higher DOS at the Fermi level for Ti₃GeC₂ than Ti₃SiC₂. This is to date not consistent with the experimental observations for bulk material, which indicate similar resistivity values for Ti₃GeC₂ and Ti₃SiC₂.¹⁴ Note, however, that the difference in calculated $DOS(E_f)$ between Ti₃SiC₂ and Ti₃GeC₂ is small. In thin film form (**Paper VI**), Ti₃GeC₂ seemingly has a higher resistivity than Ti₃SiC₂. This is likely due to the higher phase purity of the Ti₃SiC₂ thin films.

Table 3-1 Properties of MAX phases and TiC. After Barsoum¹⁴ and Emmerlich.¹⁶

Phase	Hardness (GPa)	Young's modulus (GPa)	Resistivity ($\mu\Omega\text{cm}$)	Poisson's ratio	Thermal conductivity ($\text{Wm}^{-1}\text{K}^{-1}$)
TiC	30	360	200 – 260	0.19	21
Ti ₃ SiC ₂ (bulk)	5	346	22	0.2	37
Ti ₃ SiC ₂ (thin film)	24	320	25	–	–
Ti ₃ GeC ₂ (bulk)	5	340	22	–	–

The mechanical deformation behavior of MAX phases is remarkably different from that of the hard and brittle binary carbides and nitrides. In MAX phases, the anisotropic crystal structure means that basal-plane slip is the dominant slip system. Deformation therefore occurs by kinking and delamination, rendering the MAX phase machinable and ductile. **Paper X** studies the how the deformation of Ti₃SiC₂ is affected when kinking is inhibited in a multilayer structure with TiC.

Regarding the phase stability of the MAX phases in the Ti-Si-C and Ti-Ge-C materials systems, there is a distinct difference. Both Ti₂GeC and Ti₃GeC₂ are thermodynamically stable, while there is only one stable MAX phase, Ti₃SiC₂, in the Ti-Si-C

system. One of the features of the sputtering method (see chapters 4 and 5) is the possibility to synthesize metastable phases. Our group, together with Uppsala, has previously synthesized Ti_4SiC_3 , a metastable MAX phase in the Ti-Si-C system, as well as two *intergrown structures*, $\text{Ti}_7\text{Si}_2\text{C}_5$ and $\text{Ti}_5\text{Si}_2\text{C}_3$. In these structures, one 312 unit cell is intergrown with one cell of either 413 (in $\text{Ti}_7\text{Si}_2\text{C}_5$) or 211 (in $\text{Ti}_5\text{Si}_2\text{C}_3$); a regular structure repeated over significant distances and easily detectable by X-ray diffraction. These metastable phases and structures (413, 523, and 725) all exist in the Ti-Ge-C system.¹⁷ Unlike the thermodynamically stable Ti_2GeC ; however, the hypothetical MAX phase Ti_2SiC remains elusive.¹⁸ Finally, the only thermodynamically stable MAX phase in the Ti-Sn-C system is Ti_2SnC .¹⁴ Additionally, our recent work¹⁹ has demonstrated the existence of a metastable Ti_3SnC_2 phase.

3.4 $\text{Ti}_5\text{Si}_3\text{C}_x$ and other Nowotny phases

The Nowotny phase $\text{Ti}_5\text{Si}_3\text{C}_x$ can be considered a solid solution of carbon in the silicide Ti_5Si_3 .¹⁸ Nowotny reported the existence of numerous such phases in the 1960s, e.g., $\text{Zr}_5\text{Si}_3\text{C}_x$ and $\text{V}_5\text{Ge}_3\text{C}_x$.¹² From a structural viewpoint, they are closely related with TiC and the MAX phases, in that they share the fundamental Ti_6C octahedral building block. However, in the Nowotny phases, the M_6X octahedra share faces rather than edges (as in MAX phases and binary transition-metal carbides). Their unit cell is hexagonal, and not as anisotropic as that of the MAX phases; the c and a lattice parameters of $\text{Ti}_5\text{Si}_3\text{C}_x$ are ~ 5.18 Å and ~ 7.45 Å; note that the a -axis of $\text{Ti}_5\text{Si}_3\text{C}_x$ is larger than its c -axis.¹⁸

3.5 Literature review

This section is a review on relevant previous work on thin-film synthesis of Ti-Si-C and related systems. For descriptions of the methods, see chapter 4.

3.5.1 Chemical Vapor Deposition (CVD)

There are three “classic” papers on CVD synthesis of Ti_3SiC_2 , by Nickl *et al.*,²⁰ Goto and Hirai,²¹ and Racault *et al.*²² All these studies were performed before Barsoum’s work. More recently, Pickering *et al.*²³ and Jacques *et al.*²⁴ have synthesized Ti_3SiC_2 by CVD, and Fakhri *et al.*²⁵ reported growth of $\text{Ti}_3\text{SiC}_2/\text{SiC}$ multilayers. With the exception of the last-mentioned study, the objective in these investigations is to synthesize single-phase Ti_3SiC_2 . The synthesis temperature is typically 1000 °C – 1300 °C. From these studies, it can be concluded that it is difficult to obtain phase-pure Ti_3SiC_2 by CVD. Typically, it co-exists with TiC, SiC, TiSi_2 , and/or $\text{Ti}_5\text{Si}_3\text{C}_x$, although Pickering *et al.* obtained reasonably pure material. Goto and Hirai also synthesized a significant amount of polycrystalline Ti_3SiC_2 , a plate of 40×12 mm², and obtained the high deposition rate of 200 $\mu\text{m}/\text{h}$. However, important limitations of CVD with respect to Ti_3SiC_2 synthesis are the difference in reactivity between the Ti and Si sources TiCl_4 and SiCl_4 , which leads to gas phase depletion, and silicidation of TiC, as well as etching caused by the presence of HCl.

3.5.2 Sputtering

Work on sputtering of Ti-Si-C and related materials systems takes place along two different, but related, routes, which I will refer to as “low-temperature synthesis” and “high-temperature synthesis”. I draw the line between the two in the following man-

ner: MAX phases have large and complex unit cells. This means that, normally, a significant amount of thermally activated diffusion is required for the elements to partition correctly in order to form the MAX structure. Accordingly, “high-temperature synthesis” means “high enough temperature to form MAX phases”, while “low-temperature synthesis” means the opposite. Naturally, the limit is not strict. As discussed below, numerous authors attempt to lower the required process temperature.

Apart from me and my colleagues at Linköping and Uppsala, work on sputtering of MAX carbides that falls into the “high temperature synthesis” category has been reported from Schneider’s group at RWTH-Aachen.[‡]

Most sputtering-syntheses of MAX phases have been performed at substrate temperatures in the range 800 °C – 1000 °C. In addition to the Ti-Si-C and Ti-Ge-C systems previously studied by our group,^{17,18,26} sputtering of Ti-Al-C has been performed in Uppsala, where Wilhelmsson *et al.*²⁷ synthesized Ti₂AlC and Ti₃AlC₂ using three elemental targets, and in Aachen where Walter *et al.*²⁸ synthesized Ti₂AlC using a Ti target and a Ti₂AlC target (a similar approach to what I use in **Paper II**). The group in Aachen has further synthesized Cr₂AlC and V₂AlC by sputtering from elemental targets.^{29,30} Additionally, they have demonstrated growth of Cr₂AlC by sputtering from a Cr₂AlC target at a substrate temperature as low as 450 °C, although the crystalline quality as evidenced by X-ray diffraction was not as good as that of Cr₂AlC deposited at 850 °C.³¹ It has also been demonstrated that V₂GeC can be synthesized at a substrate temperature of 450 °C.³² All these results indicate that – as a rule of thumb – there are two factors that determine what MAX phases can be synthesized at low substrate temperature. First, it is the order of MAX phase (211, 312, or 413). Larger unit cells require higher temperature to form, due to the longer diffusion length compared to smaller unit cells, and the corresponding need for thermal activation. As a general estimate, it can therefore be argued that 211 phases can be synthesized at lower temperature than 312 and 413 phases. Second, it is the factor of competing phases and how stable they are. In particular, if the binary carbide is very stable, it can be expected that the corresponding MAX phase requires a high synthesis temperature. From this point of view, it is not surprising that Cr₂AlC and V₂GeC (where the binary carbides have lower relative stability than in the TiC-based systems) can be synthesized at a relatively low substrate temperature (450 – 500 °C), that Ti₂AlC and Ti₂GeC can be grown at intermediate temperature (~700 °C), and that Ti₃SiC₂ and to an even larger extent the 413 phases require synthesis temperatures in the range 800 – 1000 °C.

Admittedly, these arguments are oversimplified – many other factors will affect MAX-phase growth. For example, the composition must be correct, and there may be several competing phases in addition to the binary carbides. But this reasoning does contain a certain kernel of truth, and is paralleled by theoretical investigations of the electronic structure of MAX phases. Sun *et al.*³³ proposed a classification of M₂AX carbides into “strongly coupled” and “weakly coupled” phases based on a systematic study of the bonding between MC and A layers. For example, the charge-density distributions of TiC and CrC are similar, but Ti₂AlC and Cr₂AlC show extensive differences due to the difference in valence-electron concentration (the elements Ti and Cr have 4 and 6 valence electrons, respectively).³³ Sun *et al.* showed that the Ti-Al bond

[‡] There are also reports on sputtering of MAX *nitrides*, from, e.g., Linköping, Rossendorf (Germany), Poitiers (France), and the University of Illinois at Urbana-Champaign. But here, I will restrict the discussion to carbides.

is much weaker than the Cr-Al bond, i.e., Cr₂AlC is “strongly coupled” and Ti₂AlC is “weakly coupled”. The difference in bonding affects properties like bulk moduli^{30,33} and shear moduli³⁴ of MAX phases. Additionally, it may explain why, e.g., Cr₂AlC can be synthesized at lower temperature than Ti₂AlC – the relative phase stability (compared to the binaries) is greatly influenced by the bonding configuration.

“Low-temperature synthesis” has been reported by several groups. Gulbinski *et al.*³⁵ synthesized Ti-Si-C using reactive sputtering at 750 °C and observed formation of Ti₃Si₃C_x but concluded that a temperature increase would be required in order to synthesize Ti₃SiC₂. Krzanowski *et al.*^{36,37} studied films deposited by rf magnetron cosputtering of TiC and SiC targets. A substrate temperature of 220-650 °C yielded films with TiC and amorphous SiC that increased the hardness compared to pure TiC coating from 10 GPa to 20-22 GPa. In comparison, the typical value for bulk TiC is 28-30 GPa. For electrical properties, these rf-sputtered films exhibited an increased electrical resistivity from 182 μΩcm to 2300 μΩcm with increasing Si content from zero to 38.3%. Zehnder *et al.*³⁸ reported reactive sputtering of Ti-Si-C on steel substrates at ~250 °C at a bias of –100 V. At this temperature, the only crystalline phase formed was TiC. In addition, SiC, (hydrogenated) C, and TiSi_x formed as amorphous phases. By varying the acetylene flux and the Si target power, they deposited films approaching 3Ti:Si:2C composition. Recently, Lopez *et al.*³⁹ investigated sputtered films in the Ti-rich corner of the Ti-Si-C composition diagram. Unsurprisingly, none of these studies showed any formation of Ti₃SiC₂, again underlining the importance of a relatively high deposition temperature in order to form this phase.

3.5.3 Cathodic arc deposition

Only very recently has cathodic arc deposition (see section 4.1.2) been employed for MAX-phase synthesis. Rosén *et al.*⁴⁰ have reported synthesis of epitaxial Ti₂AlC using a pulsed cathodic-arc setup from elemental Ti, Al, and C cathodes at a substrate temperature of 900 °C. Flink *et al.*⁴¹ have investigated Ti₂AlN synthesis by reactive cathodic arc deposition from 2Ti:Al compound cathodes. Notably, the latter study allowed deposition of Ti₂AlN at a substrate temperature of 500 °C, ~200° lower than has been reported for sputtering of Ti₂AlN. This indicates that the high degree of ionization (almost 100 % for any species) of the deposition flux in cathodic arc deposition may provide the control of ion energy necessary to substantially decrease the deposition temperature (compared to sputtering) for MAX phases.

3.5.4 Pulsed laser deposition (PLD)

The idea of using PLD for MAX-phase synthesis is very good: since the method produces species with significantly higher energy than sputtering does and has the ability to maintain even very complicated target stoichiometries, PLD has the potential to lower the process temperature for MAX-phase synthesis and to permit synthesis using a single MAX-phase target. For these reasons, it is quite surprising that only a few studies exist on the subject.

Phani *et al.*⁴² synthesized Ti-Si-C films in the temperature range 25 °C – 600 °C predominantly consisting of TiC and amorphous phases. Of particular interest are their results on mechanical properties, where they performed nanoindentation and subsequent AFM imaging and observed no cracking around the indents. This is an indication of a ductile behavior very similar to what I observe in **Paper III**. Further, they

observed an unidentified peak in XRD for the films deposited on steel substrates at 25 °C, 200 °C, and 400 °C, and speculated that this could be due to Ti_3SiC_2 formation caused by diffusion of carbon into the steel substrate, thus achieving the correct stoichiometry for Ti_3SiC_2 . However, they pointed out several inconsistencies with this speculation; primarily that the peak is *not* present at 600 °C, where more diffusion is expected. Further, the peak is present at 25 °C, where diffusion is very limited, and finally, the specified peak position does not fit very well to any Ti_3SiC_2 peak. Consequently, the other explanation that Phani *et al.* proposed is more likely; the peak can probably be attributed to retained austenite in the substrate. In a subsequent study,⁴³ they varied the stoichiometry, in particular the C content, of Ti-Si-C films using the hybrid method magnetron sputtering-PLD (MSPLD). A high C content (55 %) resulted in films with low friction against steel with a friction coefficient of 0.1 – 0.4 while maintaining high hardness (28 GPa) and good wear resistance. Hu *et al.*⁴⁴ synthesized Ti-Si-C films using PLD and a Ti_3SiC_2 target at substrate temperatures of 100 °C – 300 °C. The films exhibited promising mechanical properties with friction coefficient down to 0.2. The controversy in this paper is the phase identification, where Hu *et al.* attribute two X-ray diffraction peaks to the 102 and 008 peaks of Ti_3SiC_2 . These peaks, however, also fit the TiC 111 and 200 peaks,⁴⁵ and most likely Hu *et al.* did not synthesize Ti_3SiC_2 , but a nanocomposite TiC-based material similar to that reported by Zehnder *et al.*,³⁸ Phani *et al.*,⁴² and myself (**Paper III**).

To conclude the discussion on PLD synthesis of Ti-Si-C materials, the method has some unique attributes that, in principle, provide the possibility to synthesize Ti_3SiC_2 at low temperatures, and this has been attempted by some authors. No unambiguous evidence of Ti_3SiC_2 formation in PLD films has been presented. This does not change the fact that the method has great potential and, in the future, could provide an important alternative to sputtering.

-
- ¹ P. Villars, A. Prince, and H. Okamoto (editors) *Handbook of ternary alloy phase diagrams* ASM International, Metals Park, OH (1995)
- ² J. C. Viala, N. Peillon, F. Bosselet, and J. Bouix *Phase equilibria at 1000 °C in the Al-C-Si-Ti quaternary system: an experimental approach* Materials Science and Engineering A 229 95 (1997)
- ³ W. J. J. Wakelkamp, F. J. J. van Loo, and R. Metselaar *Phase relations in the Ti-Si-C system* Journal of the European Ceramic Society 8 135 (1991)
- ⁴ M. Touanen, F. Teyssandier, and M. Ducarroir *Theoretical approach to chemical vapour deposition in the atomic system Ti-Si-C-Cl-H* Journal of Materials Science Letters 8 98 (1989)
- ⁵ S. Sambasivan and W. T. Petuskey *Phase relationships in the Ti-Si-C system at high pressures* Journal of Materials Research 7 1473 (1992)
- ⁶ L. E. Toth *Transition metal carbides and nitrides* Academic Press (1971)
- ⁷ W. S. Williams *Physics of transition metal carbides* Materials Science and Engineering A105/106 1 (1988)
- ⁸ H. O. Pierson *Handbook of refractory carbides and nitrides* Noyes Publications (1996)
- ⁹ W. S. Williams *Transition metal carbides* Progress in Solid State Chemistry 6 57 (1971)
- ¹⁰ H. Högberg *Low-temperature deposition of epitaxial transition metal carbide films and Superlattices using C₆₀ as carbon source* Ph. D. Thesis, Acta Universitatis Upsaliensis no. 507, ISBN 91-554-4645-0 Uppsala University (2000)
- ¹¹ W. Jeitschko and H. Nowotny *Die Kristallstruktur von Ti₃SiC₂ – ein neuer Komplexcarbidge-Typ* Monatshefte für Chemie 98 329 (1967)
- ¹² H. Nowotny *Strukturchemie einiger verbindungen der übergangsmetalle mit den elementen C, Si, Ge, Sn* Progress in Solid State Chemistry 2 27 (1970)
- ¹³ G. Hägg *Metalliska nitrid, karbider, borider, och hydrid* Teknisk tidskrift för bergsvetenskap 4 23 (1931) Accessible in digital format at <http://runeberg.org/tektid> (March 10, 2007)
- ¹⁴ M. W. Barsoum *The M_{n+1}AX_n-Phases: a new class of solids* Progress in Solid State Chemistry 28 201 (2000)
- ¹⁵ Y. Zhou, Z. Sun, X. Wang, and S. Chen *Ab initio geometry optimization and ground state properties of layered ternary carbides Ti₃MC₂ (M=Al, Si and Ge)* Journal of Physics: Condensed Matter 13 10001-10010 (2001)
- ¹⁶ J. Emmerlich *MAX Phase Thin Films; Unique Multifunctional Ceramics with the Elements Ti, Si, Ge, Sn, and C* Ph. D. Thesis, Linköping Studies in Science and Technology no. 1024, ISBN 91-85523-64-X, Linköping University (2006)
- ¹⁷ H. Högberg, P. Eklund, J. Emmerlich, J. Birch, and L. Hultman *Epitaxial Ti₂GeC, Ti₃GeC₂, and Ti₄GeC₃ MAX-phase thin films grown by magnetron sputtering* Journal of Materials Research 20 779 (2005)
- ¹⁸ J.-P. Palmquist, S. Li, P. O. Å. Persson, J. Emmerlich, O. Wilhelmsson, H. Högberg, M. I. Katsnelson, B. Johansson, R. Ahuja, O. Eriksson, L. Hultman, and U. Jansson *New MAX phases in the Ti-Si-C system studied by thin film synthesis and ab initio calculations* Physical Review B 70 165401 (2004)
- ¹⁹ H. Högberg, J. Emmerlich, P. Eklund, O. Wilhelmsson, J.-P. Palmquist, U. Jansson, and L. Hultman *Growth and property characterization of epitaxial MAX-phase thin films from the Ti_{n+1}(Si,Ge,Sn)C_n systems* Proceedings of the 11th International Ceramics Congress, Acireale, Sicily, Italy, June 4-9, Advances in Science and Technology 45 2648 (2006)
- ²⁰ J. Nickl, K. K. Schweitzer, and P. Luxenburg *Gasphasenabscheidung im system Ti-Si-C* Journal of the Less-Common Metals 26 335 (1972)
- ²¹ T. Goto and T. Hirai *Chemically vapor deposited Ti₃SiC₂* Materials Research Bulletin 22 1195 (1987)
- ²² C. Racault, F. Langlais, R. Naslain, and Y. Kihn *On the chemical vapour deposition of Ti₃SiC₂ from TiCl₄-SiCl₄-CH₄-H₂ gas mixtures Part II: An experimental approach* Journal of Materials Science 29 3941 (1994)
- ²³ E. Pickering, W. J. Lackey, and S. Crain *CVD of Ti₃SiC₂* Chemical Vapor Deposition 6 289 (2000)
- ²⁴ S. Jacques, H. Di-Murro, M. -P. Berthet, and H. Vincent *Pulsed reactive chemical vapor deposition in the C-Ti-Si system from H₂/TiCl₄/SiCl₄* Thin Solid Films 478 13 (2005)
- ²⁵ H. Fakhri, S. Jacques, M.-P. Berthet, F. Bosselet, O. Dezellus, and J.-C. Viala *The growth of Ti₃SiC₂ coatings onto SiC by reactive chemical vapor deposition using H₂ and TiCl₄* Surface and Coatings Technology 201 3748 (2006)

- ²⁶ J. Emmerlich, J.-P. Palmquist, H. Högberg, J. M. Molina-Aldareguia, Zs. Czirány, Sz. Sasvári, P. O. Å. Persson, U. Jansson, and L. Hultman *Growth of Ti₃SiC₂ thin films by elemental target magnetron sputtering* Journal of Applied Physics 96 4817 (2004)
- ²⁷ O. Wilhelmsson, J. -P. Palmquist, T. Nyberg, and U. Jansson *Sputtering of Ti₂AlC and Ti₃AlC₂ thin films* Applied Physics Letters 85 1066 (2004)
- ²⁸ C. Walter, C. Martinez, T. El-Raghy, and J. Schneider *Towards large area MAX phase coatings on steel* Steel Research International 76 225 (2005)
- ²⁹ R. Mertens, Z. Sun, D. Music, and J. Schneider *Effect of the composition on the structure of Cr-Al-C investigated by combinatorial thin film synthesis and ab initio calculations* Advanced Engineering Materials 6 903 (2004)
- ³⁰ J. M. Schneider, R. Mertens, and D. Music *Structure of V₂AlC studied by theory and experiment* Journal of Applied Physics 99 013501 (2006)
- ³¹ C. Walter, D. P. Sigumonrong, T. El-Raghy, and J. M. Schneider *Towards large area deposition of Cr₂AlC on steel* Thin Solid Films 515 389 (2006)
- ³² O. Wilhelmsson, P. Eklund, H. Högberg, L. Hultman, and U. Jansson (unpublished)
- ³³ Z. Sun, D. Music, R. Ahuja, S. Li, and J. M. Schneider *Bonding and classification of nanolayered ternary carbides* Physical Review B 70 092102 (2004)
- ³⁴ D. Music, Z. Sun, A. A. Voevodin, and J. M. Schneider *Electronic structure and shearing in nanolaminated ternary carbides* Solid State Communications 139 139 (2006)
- ³⁵ W. Gulbinski, A. Gilewicz, T. Suszko, B. Warcholinski, and Z. Kuklinski *Ti-Si-C sputter deposited thin film coatings* Surface and Coatings Technology 180-181 341 (2004)
- ³⁶ J. E. Krzanowski and S. H. Koutzaki *Mechanical properties of sputter-deposited Titanium-Silicon-Carbon films* Journal of the American Ceramic Society 84 672 (2001)
- ³⁷ S. H. Koutzaki, J. E. Krzanowski, and J. J. Nainapampil *Structure and mechanical properties of Ti-Si-C coatings deposited by magnetron sputtering* Journal of Vacuum Science and Technology A 19(4) 1912 (2001)
- ³⁸ T. Zehnder, J. Matthey, P. Schwaller, A. Klein, P. -A. Steinmann, and J. Patscheider *Wear protective coatings consisting of TiC-SiC-a-C:H deposited by magnetron sputtering* Surface and Coatings Technology 163-164 238 (2003)
- ³⁹ C. Lopez, N. M. G. Parreira, S. Carvalho, A. Cavaleiro, J. P. Rivière, E. Le Bourhis, and F. Vaz *Magnetron sputtered Ti-Si-C thin films prepared at low temperatures* Surface and Coatings Technology (in press, 2007)
- ⁴⁰ J. Rosén, L. Ryves, P. O. Å. Persson, and M. M. M. Bilek *Deposition of epitaxial Ti₂AlC thin films by pulsed cathodic arc* Journal of Applied Physics 101 056101 (2007)
- ⁴¹ A. Flink, J. Sjöln, L. Karlsson, and L. Hultman *MAX-Phase Ti₂AlN coatings by arc deposition* (in manuscript, 2007)
- ⁴² A. R. Phani, J. E. Krzanowski, and J. J. Nainapampil *Structural and mechanical properties of TiC and Ti-Si-C films deposited by pulsed laser deposition* Journal of Vacuum Science and Technology A 19(5) 2252 (2001)
- ⁴³ J. E. Krzanowski, J. J. Nainapampil, and A. R. Phani *Mechanical and tribological properties of sub- and superstoichiometric Ti-C and Ti-Si-C films deposited by magnetron sputtering-pulsed laser deposition* Journal of Vacuum Science and Technology A 21(6) 1829 (2003)
- ⁴⁴ J. J. Hu, J. E. Bultman, S. Patton, and J. S. Zabinski *Pulsed laser deposition and properties of M_{n+1}AX_n phase formulated Ti₃SiC₂ thin films* Tribology Letters 16 113 (2004)
- ⁴⁵ P. Eklund, J. -P. Palmquist, O. Wilhelmsson, U. Jansson, J. Emmerlich, H. Högberg, and L. Hultman *Comment on "Pulsed laser deposition and properties of M_{n+1}AX_n phase formulated Ti₃SiC₂ thin films"* Tribology Letters 17 977 (2004)

4 Thin-film synthesis

“-Ippon waza ni meijin nashi” (“No master is limited to one technique”)

Kyozo Mifune, 10th Dan

This chapter contains a brief introduction to sputtering, the synthesis method used in this work, and further discusses other methods that have been used to synthesize Ti-Si-C and related thin films, focusing on their attributes of interest to the present work. A more detailed discussion of sputtering can be found in chapter 5.

4.1 Physical Vapor Deposition (PVD)

4.1.1 Sputtering

In sputtering methods,¹ the solid source material (known as the *target*) is bombarded with highly energetic ions (often Ar^+) in vacuum. Source atoms are then removed from the target and move to the object to be coated (the *substrate*) where they condense to form thin films.

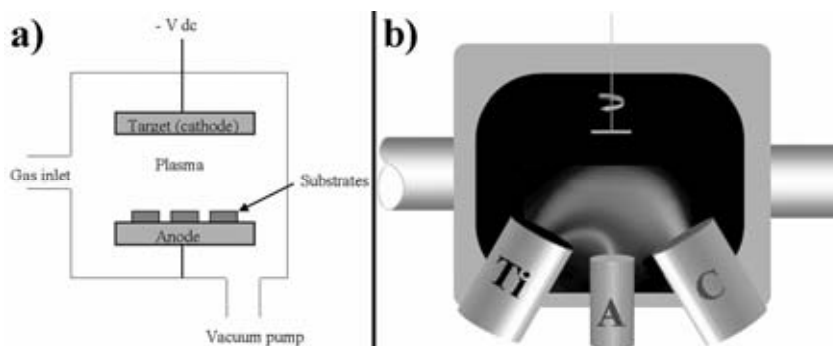


Figure 4.1 Schematic drawings of (a) a simplified sputtering system, and (b) the sputtering setup used in this work, with the three-target configuration employed in Papers I, IX, and X.

Before going into the details (chapter 5), studying a simple overview of the process is useful. Figure 4.1(b) shows a schematic drawing of a sputtering system. This basic

sputtering setup is called *diode sputtering*.^{*} The vacuum is typically ultrahigh vacuum (UHV, $\sim 10^{-9}$ mbar) in a research system, while in industrial production high vacuum (HV, $\sim 10^{-6}$ mbar) is common. The target is connected to a negative dc voltage supply (or an rf supply). The substrate holder is in front of the target. The holder may be electrically biased, grounded or floating, as well as heated or cooled. A sputtering gas, usually Ar, but sometimes another noble gas, is introduced with a pressure in the range of 10^{-3} mbar to 10^{-1} mbar. In this gas, a *glow-discharge plasma* can be initiated and maintained. A plasma is, in simple terms, a partially ionized gas (see section 5.1.1). When a plasma is present, positive (Ar^+) ions bombard the target and remove mainly neutral target atoms by momentum transfer; these atoms condense into thin films when reaching the substrate.

Figure 4.1(b) shows a schematic drawing of the sputtering setup[†] used in most of this work. The configuration shown in Figure 4.1(b) is the three-target configuration employed in **Papers I, IX, and X**, with a Ti target, an A-element (Si) target and a C (graphite) target. In **Papers II-V**, a compound target of Ti_3SiC_2 bulk material was used. The experiments in **Papers IV and V** were performed in other (high-vacuum) deposition systems.

4.1.2 Cathodic arc deposition

A characteristic of sputtering (see also section 5.1) is that the target operates in the high-voltage, low-current regime (typically ~ 500 V, $0.01 - 0.1$ A/cm²). An increased current leads to an avalanche effect that causes a low-voltage, high-current (typically ~ 10 V, $50-100$ A/cm²) *arc discharge*. This is the mode of operation for cathodic arc deposition.^{1,2} When an arc is initiated, a small cathode spot (typically < 100 μm) is formed and carries the discharge. The current density in the cathode spot is extremely high, leading to erosion by melting and evaporation as well as ejection of molten and solid particles. The locally very high power density creates a highly ionized plasma. The arc is then steered on the cathode surface to achieve homogeneous erosion.

As a consequence of the physics of arc discharges, cathodic arc deposition[‡] has some important attributes. Unlike in sputtering plasmas, the deposition flux in arc plasmas is highly ionized; the degree of ionization is close to 100 %. This offers a means of process control by applying electric and magnetic fields to guide the deposition flux and control the ion-energy distributions. A drawback with cathodic arc deposition is the presence of macroparticles ejected from the cathode. There are, however, approaches to filter out such macroparticles.

There are some recent reports on cathodic arc deposition of MAX-phase synthesis that have shown promising results; however, these investigations are still in their infancy (for further discussion, see section 3.5.3).

^{*} In practice, the basic diode-sputtering setup is rarely used today; it has been virtually completely replaced by magnetron sputtering (see section 5.2)

[†] Named “Laura”, after Laura Macahan in the TV series *How The West Was Won*

[‡] Often, especially in industry, the technique is simply referred to as *arc evaporation*. However, the more stringent term is *cathodic arc deposition*, since there are also *anodic arcs*.

4.1.3 Pulsed laser deposition (PLD)

The concept behind PLD,^{3,4} also known as laser ablation, is similar to that of sputtering. It takes place in vacuum where a solid target is vaporized. Just like in sputtering, source atoms are then removed from the target and condense at the substrate. The difference is in the method of vaporization. PLD uses a high-energy laser rather than ion bombardment to vaporize the target material.

In comparison to sputtering, PLD produces species with significantly higher energy than sputtering does and has the ability to maintain even very complicated target stoichiometries. Species condensed on the substrate are subsequently bombarded by high-energy particles, providing a large amount of energy to the growing film. These attributes are relevant for potential MAX-phase synthesis using PLD (for further discussion, see section 3.5.4).

4.2 Chemical Vapor Deposition (CVD)

CVD⁵ is different from PVD in that the material to be deposited is provided by gases that react with each other, rather than by a solid source material, which is vaporized. Typical characteristics of CVD are that it normally operates at comparatively elevated temperature and at thermodynamic equilibrium (as opposed to sputtering, which operates far from equilibrium). Its advantages include that, unlike sputtering and PLD, it is not restricted to line-of-sight deposition and, consequently, that complicated geometries can be readily coated. For a survey of CVD of Ti-Si-C thin films, see section 3.5.1.

-
- ¹ J. M. Vossen and W. Kern (editors) *Thin Film Processes II* Academic Press, San Diego, CA (1991)
- ² A. Anders *Metal plasma immersion ion implantation and deposition: a review* Surface and Coatings Technology 93 158 (1997).
- ³ D. B. Chrisey and G. K. Hubler (editors) *Pulsed Laser Deposition of Thin Films* Wiley (1994)
- ⁴ R. M. Gilgenbach, S. D. Kovaleski, J. S. Lash, L. -K. Ang, and Y. Y. Lau *Science and Applications of Energy Beam Ablation* IEEE Transactions on Plasma Science 27 150 (1999)
- ⁵ M. Ohring *The Materials Science of Thin Films* Academic Press, San Diego, CA (1992)

5 Sputtering

“We’re goin’ ballistic Mav. Go get him!!!”

Goose (Anthony Edwards), to Maverick (Tom Cruise), in “Top Gun”

Chapter 4 gave a brief introduction to sputtering and other thin-film synthesis methods. This chapter discusses the physics of sputtering in more detail. Magnetron sputtering, the method employed in this work, is described in section 5.2.

5.1 The physics of sputtering

5.1.1 What is a plasma?

All sputtering methods are plasma-based. To understand sputtering, it is therefore necessary to know what a plasma is and how it is initiated and maintained. A definition is:

Plasma is a partially ionized gas, which is electrically neutral when averaged over all particles in the plasma.

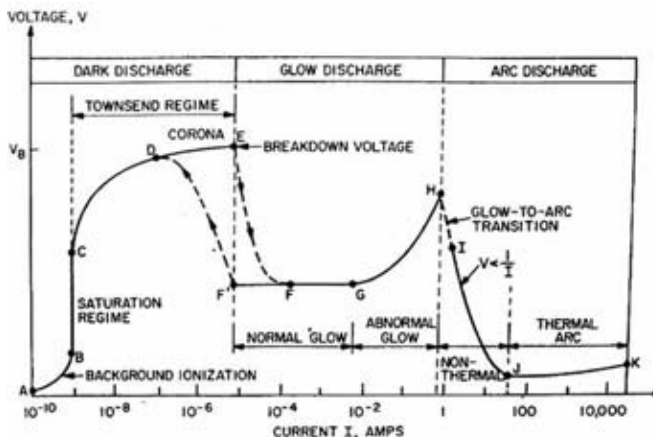


Figure 5.1 The different regimes in plasmas relevant to sputter deposition. From Roth.¹

The plasmas used in sputtering are often called *glow discharges* (or *glow-discharge plasmas*).² The situation is shown in Figure 5.1. To form plasma in a low-pressure gas, a dc voltage* is applied from a high-impedance power supply. At first, very little current flows since there are very few ions and electrons available. The current is nearly constant since all the charge present is moving. As the voltage increases, the charged particles receive enough energy to produce more charged particles by collisions with the electrodes† and with neutral gas atoms. While the current increases, the voltage is limited by the output impedance of the power supply and remains constant. Typically, the voltage can be around 600 V while the current density increases from 10^{-15} to 10^{-6} A/cm². This region is called the *Townsend discharge*.

Eventually, ions strike the cathode and release secondary electrons, a process that results in formation of more ions when secondary electrons collide with neutral gas atoms. These ions return to the cathode, produce more electrons that in turn produce more ions. In other words, an avalanche occurs. When the number of electrons generated is just enough to produce the required ions to regenerate the same number of electrons, the plasma is self-sustaining. There is a voltage drop, the current rises abruptly (typically to 10^{-2} A/cm²), and the gas begins to glow. This is known as the *normal glow* region.

When the ion bombardment has built up to cover the entire cathode surface, any further increase in power produces increases in both voltage and current density to ~800 V and ~0.1 A/cm². This region, the *abnormal discharge*, is the mode employed in sputtering processes.

If the current rises even further, a second avalanche due to thermionic electrons follows. This causes a low-voltage, high-current (typically ~10 V, 50-100 A/cm²) *arc discharge*. In sputtering processes, this arc is an unwanted nuisance and care should be taken to avoid it. Cathodic arc deposition (see section 4.1.2), on the other hand, takes advantage of the arcing.

5.1.2 The plasma, floating, and bias potentials

Any material body (e.g., a substrate) immersed in plasma (unless it is grounded or biased) will acquire a potential slightly negative with respect to ground. This is known as the *floating potential*, which arises because the electrons in the plasma have a higher mobility than the ions. Hence, more electrons than ions reach the substrate surface. For the same reason, the plasma itself is at a positive potential. If the substrate is negatively biased, the negative bias simply replaces the floating potential. However, if the substrate is positively biased, there is a very large electron flow to the substrate resulting in a large substrate heating and nonuniform current distribution. Hence, positive bias should usually (but not necessarily) be avoided.

5.1.3 The sputtering yield

The *sputtering yield* is an essential parameter in sputtering. It is the number of atoms ejected from the target surface per incident ion. It depends on the target material and the plasma properties and is determined empirically, although there are reasonable

* A radio-frequency ac voltage can also be used, but this will not be treated here.

† In a sputtering system, the target is the cathode and the substrate is the anode. The chamber walls also act as anode.

theoretical estimates.³ Values of the sputtering yield can be anything from well below 0.1 up to 5-10. It is generally desired to have a high sputtering yield, since the process will be more efficient. Among other things, the sputtering rate (and by consequence the deposition rate) will be higher. Typical sputtering-yield values are ~0.1 for C (i.e., a very low value) and ~0.5 for Ti and Si (in Ar at 500 eV).² In comparison, easily-sputtered elements like Au, Ag, Pd, Cu, and Bi have sputtering yields in Ar at 500 eV in the range 2 – 6. A closely related parameter is the *differential sputtering yield*, i.e., the sputtering yield per unit solid angle. The differential sputtering yield is important because the angular distributions of sputtered species can be very different depending on, e.g., sputtering gas and the material and microstructure of the target. Such differences can be very important when sputtering from compound targets (**Papers II-V**).

5.1.4 Transport of sputtered species

The sputtered species are ejected from the target with an energy and angular distribution, which depends on process parameters such as sputtering gas, target material, and target voltage. However, not all of the sputtered species actually arrive at the substrate; many are lost during transport. The transport phase is therefore important to any sputter-deposition process. The basic concept behind the understanding of gas-phase transport⁴ is the *mean free path*

$$\lambda_{1,2} = \frac{4kT}{\pi(d_1 + d_2)^2 P_2 (1 + \frac{M_1}{M_2})^{1/2}}, \quad (5.1)$$

where $\lambda_{1,2}$ is the mean free path of gas 1 in gas 2 (i.e., the mean free path of gas 1 colliding with molecules of gas 2), d_1 , M_1 , d_2 , and M_2 are the respective molecular diameters and masses of the two gases, P_2 is the partial pressure of gas 2, k is Boltzmann's constant, and T is the temperature.

Equation (5.1) is valid for *random* motion and shows that the mean free path depends on the respective molecular diameters and masses of the sputtering gas and the sputtered species. Assuming room temperature (300 K), equation (5.1) gives values of ~5 cm and ~22 cm for the mean free paths of Ti and C, respectively, in Ar at a pressure of 2 mTorr.

In a sputtering process, the species have an initial kinetic energy that should be taken into account for quantitative analyses.⁵ Some of this kinetic energy will be lost in each collision with sputtering-gas molecules; after sufficiently many collisions, the sputtered species will have lost all of their initial kinetic energy. Consequently, the transport of sputtered species is categorized into three regimes: the *ballistic* regime, where sputtered atoms travel in straight paths from the target without suffering collisions; a transition regime, where the sputtered atoms have undergone some collisions but still retain some of their initial energy; and a *thermalized* (or diffusive) regime, where all of the initial energy of the sputtered species has been lost and the motion of the species is random (thermal).

The target-to-substrate distance in sputtering systems is typically of the order of 10 cm, the same order of magnitude as the mean free paths calculated above. Consequently, sputtered species can be ballistic, thermalized, or in the transition regime de-

pending on process-specific parameters such as geometry, sputtering-gas pressure, and target material. Usually, a fully thermalized deposition flux is detrimental to film properties, as the beneficial effects of the kinetic energy of the species are lost. On the other hand, the low sputtering-gas pressure required to remain in the fully ballistic regime is often associated with low sputtering rate.[‡] Therefore, in practice, most sputtering processes operate in the transition regime (the pressure is typically in the range 3 – 6 mTorr). Note, however, that there are important differences between species. Light and small species (e.g., C) will have longer mean free paths than heavier and larger species (e.g., Ti). Correspondingly, transport of C will be fully ballistic at higher pressures than transport of Ti. On the other hand, once in the transition regime, C atoms are much more affected by each collision than Ti atoms. These effects can be important to compound-target sputtering (see, e.g., **Paper II**).

5.1.5 Effects at the substrate

After the processes described in the previous sections, the sputtered species reach the substrate. However, several issues remain to be accounted for.²

First, the probability that an atom condenses on the substrate, i.e., the *sticking coefficient*, may be lower than unity. Often, the sticking coefficient is *assumed* to be unity, since it is very difficult to determine and the assumption tends to give correct results. For volatile species, however, this assumption is not valid. A practically useful qualitative indication of whether variations in sticking coefficient affect the film composition is that such variations result in a temperature-dependent, but *not* pressure-dependent film composition.

Second, *resputtering* may occur. Species condensed on the substrate can be resputtered by sputtering-gas ions or by energetic neutrals backscattered from the target. The former effect is particularly important when high bias voltages are applied to the substrate. Bias is normally applied to increase the ion bombardment and provide additional energy to the growing film (e.g., to improve the film density); however, if the bias is too high, the resputtering effect can be seriously detrimental. Resputtering by energetic neutrals is especially important if the target contains heavy elements. When sputtering-gas (e.g., Ar) ions bombard the target, there is a probability (backscattering yield) that they will be backscattered as neutral atoms.[§] The backscattered Ar neutrals will have a kinetic energy similar to that of the incident Ar ion, whose energy is determined by the target voltage (e.g., a target voltage of –500 V gives an incident-ion energy of 500 eV). If a large fraction of the incident Ar ions are backscattered, energetic Ar neutrals will bombard the growing film and affect its composition and microstructure. A typical example is W-Ti films,⁶ where the presence of the heavy element W in the target leads to large amount of backscattered Ar neutrals. On the other hand, the lighter element Ti is much more prone to resputtering than W; resulting in Ti-deficient films.

[‡] Sometimes, the required pressure to remain in the ballistic regime may be even so low that the plasma cannot be sustained.

[§] The neutralization process is called *Auger neutralization*.

5.2 Magnetron sputtering

5.2.1 dc magnetron sputtering

This type of sputtering is widespread in both research facilities and industrial production, and is the synthesis method I have used in this work. One reason for the industrial interest is the possibility to get a higher deposition rate than in diode sputtering. The central idea is to use a magnetic field to confine electrons near the target, in order to achieve a higher sputtering rate.

Let us start by studying what happens when a magnetic field \mathbf{B} is superimposed on the electric field \mathbf{E} between the target and the substrate. The electrons are subject to the Lorentz force

$$\mathbf{F} = m \frac{d\mathbf{v}}{dt} = e(\mathbf{E} + \mathbf{v} \times \mathbf{B}), \quad (5.2)$$

where e is the electronic charge, m the electron mass and \mathbf{v} the electron velocity. If \mathbf{E} and \mathbf{B} are parallel and the electrons are launched in their direction, $\mathbf{v} \times \mathbf{B}$ vanishes and the electrons are simply accelerated by the \mathbf{E} -field from the cathode to the anode. If the electrons are launched at an angle to the \mathbf{E} - and \mathbf{B} -fields, they will move in a corkscrew fashion. Generally, the magnetic field prolongs the electron residence time in the plasma, enhancing the ionization probability. This means that more Ar^+ ions will be available to sputter target atoms, resulting in a higher sputtering rate.

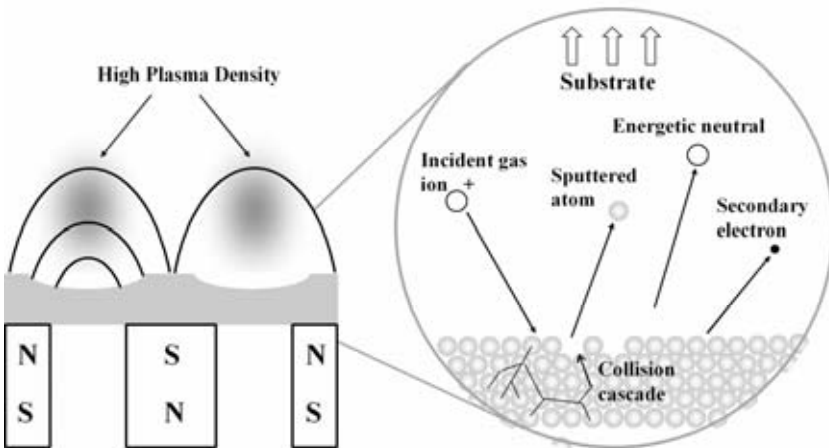


Figure 5.2 Schematic drawing of (left) a magnetron, and (right) processes occurring at the target surface.

The *magnetron* is a device where the magnetic field is applied parallel to the target and perpendicular to the electric field. The situation is shown schematically in Figure 5.2. Ideally, electrons never reach the anode but are trapped near the target, enhancing the ionization efficiency there, i.e., the presence of secondary electrons increases the number of incident gas ions. When the electrons are first emitted from the target, they move in a helix towards the anode. As they encounter the \mathbf{B} -field, they are bent back

in an orbit to the target. By solving the Lorentz equation (6.1) the equations of motion of the electrons are

$$y = \frac{qE}{m\omega_c^2}(1 - \cos \omega_c t) ; x = \frac{Et}{B} \left(1 - \frac{\sin \omega_c t}{\omega_c t}\right), \quad (5.3)$$

where x and y are the distances along and above the target, and ω_c is the cyclotron frequency qB/m . These equations describe a cycloidal motion near the cathode, where both \mathbf{E} and \mathbf{B} are present. By orienting \mathbf{B} suitably, a region known as a *race-track* can be defined. There, the electrons move around at high speed, efficiently ionizing the working gas. Sputtering is most intense in the race-track region, resulting in a characteristic erosion profile on the target.

5.2.2 High-power impulse magnetron sputtering (HIPIMS)

A recent innovative PVD approach is to employ a pulsed high-power supply rather than a dc or rf power supply to the target.⁷ This technique, originally developed at Linköping University,⁸ is known as high-power impulse magnetron sputtering (HIPIMS).^{**} In **Paper V**, HIPIMS was employed to deposit Ti-Si-C thin films from a Ti₃SiC₂ target.

A simple way of viewing HIPIMS is as a sputtering technique that emulates cathodic arc deposition, and – ideally! – has the advantages of both sputtering and cathodic arc deposition, but without their respective disadvantages. The high-power pulses applied to the target yield a highly ionized deposition flux similar to that obtained in cathodic arc deposition.^{††} Thus, HIPIMS allows control of the deposition flux and the ion-energy distributions process through applied electric and magnetic fields, just like cathodic arc deposition does. Unlike the latter technique, however, HIPIMS does not suffer from macroparticles ejected from the cathode. A remaining issue with HIPIMS is the low deposition rate compared to dc magnetron sputtering and cathodic arc deposition;⁷ this issue is subject to intense development efforts from both industry and academia.

^{**} The technique is also known as high-power pulsed magnetron sputtering (HPPMS).

^{††} There are other methods than cathodic arc deposition and HIPIMS to achieve a highly ionized deposition flux. Some examples are magnetron sputtering using inductively coupled plasmas or electron cyclotron resonance discharges. The family of PVD techniques with ionized deposition flux is referred to as Ionized Physical Vapor Deposition (IPVD) techniques; see the review by Helmersson *et al.*⁷

-
- ¹ J. R. Roth *Industrial Plasma Engineering Volume 1: Principles* Institute of Physics, Bristol (1995)
- ² J. M. Vossen and W. Kern (editors) *Thin Film Processes II* Academic Press, San Diego, CA (1991)
- ³ M. Ohring *The Materials Science of Thin Films* Academic Press, San Diego, CA (1992)
- ⁴ A. Roth *Vacuum Technology* Elsevier, Amsterdam (1990)
- ⁵ S. M. Rossnagel, I. Yang, and J. J. Cuomo *Compositional changes during magnetron sputtering of alloys* Thin Solid Films 199 59 (1991)
- ⁶ L. R. Shaginyan, M. Misina, S. Kadlec, L. Jastrabik, A. Mackova, and V. Perina *Mechanism of the film composition formation during magnetron sputtering of WTi* Journal of Vacuum Science and Technology A 19(5) 2554 (2001)
- ⁷ U. Helmersson, M. Lattemann, J. Bohlmark, A. P. Ehasarian, and J. T. Gudmundsson *Ionized Physical Vapor Deposition (IPVD): A review of technology and applications* Thin Solid Films 513 1 (2006)
- ⁸ V. Kouznetsov, K. Macák, J. M. Schneider, U. Helmersson, and I. Petrov *A novel pulsed magnetron sputter technique utilizing very high target power densities* Surface and Coatings Technology 122 290 (1999)

6 Thin-film growth

-"Happiness is neither virtue nor pleasure nor this thing nor that but simply growth. We are happy when we are growing."

William Butler Yeats

The two previous chapters discussed thin-film deposition processes, particularly sputtering. This chapter deals with what happens once the sputtered species have condensed on the substrate, i.e., *thin-film growth*.

6.1 Nucleation and growth

In sputter-deposition, species arrive at the substrate surface with kinetic energies of the order of a few electron volts. Subsequently, these adatoms diffuse on the surface to energetically favorable sites, e.g., kinks, steps, or existing clusters of deposited atoms.¹ The formation of adatom clusters leads to *nucleation* once the clusters reach a critical size.* Nucleation theory² differs between homogeneous nucleation, where the probability to form a nucleus is the same everywhere, and heterogeneous nucleation, where nucleation is more probable on heterogeneities like interfaces, surfaces, and steps.³ Therefore, in thin-film growth, nucleation is always heterogeneous.

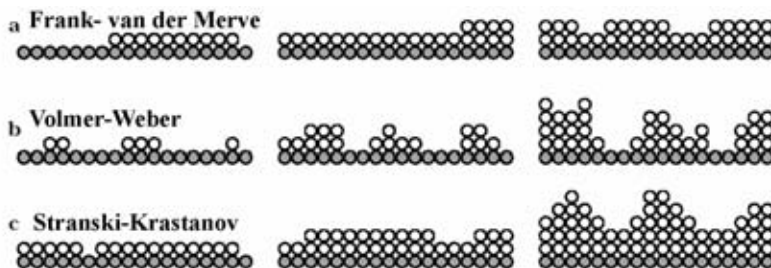


Figure 6.1 Schematic illustration of (a) Frank-van der Merve growth, (b) Volmer-Weber growth, and (c) Stranski-Krastanov growth.

* Nucleation is more fascinating phenomenon than it may seem at first sight. A nucleation event in a closed equilibrium system corresponds to a decrease in the entropy, which would be a violation of the second law of thermodynamics. This can be understood from the theory of fluctuations in equilibrium systems; nucleation is possible because of statistical entropy fluctuations. As the critical nucleus size is small, the activation barrier (decrease in entropy) that must be overcome to form stable nuclei is of the order of Boltzmann's constant.

The initial stage of film growth is ideally classified into three characteristic modes: *Frank-van der Merve* (F-M) or layer-by-layer growth, *Volmer-Weber* (V-W) or island growth, and *Stranski-Krastanov* (S-K) or initial layer growth followed by island growth. These three growth modes are schematically illustrated in Figure 6.1. During epitaxial growth (see section 6.2), F-M is often the operative growth mode, while V-W growth usually occurs in polycrystalline film growth (see section 6.3). S-K growth can occur in heteroepitaxy (see section 6.2).

6.2 Epitaxial film growth

The term *epitaxy* (from the Greek words *epi*, placed or resting upon, and *taxis*, arrangement) can be defined as extended single-crystal film formation on top of a crystalline substrate.¹ Epitaxy occurs when it is energetically favorable for the deposited species to crystallographically align with the substrate in order to minimize the total interfacial energy. There are two different types of epitaxy, *homoepitaxy*, where the film and the substrate are the same material, and *heteroepitaxy*, where the two materials are different.

Homoepitaxy is often used in the semiconductor industry to deposit, e.g., Si on Si, in order to grow an epitaxial layer with fewer defects and higher purity than the substrate. **Paper I** deals with homoepitaxy of Ti_3SiC_2 on bulk Ti_3SiC_2 substrates. In **Paper I**, the substrates are polycrystalline; the use of the word *epitaxy* in this context refers to the growth of a Ti_3SiC_2 thin film epitaxially related to an individual grain in the substrate, rather than extended single-crystal thin-film growth.[†] In **Papers II** and **VI-X**, I investigate heteroepitaxially grown TiC_x and Ti_3SiC_2 , as well as epitaxial TiC/SiC and TiC/ Ti_3SiC_2 multialyers. These studies were predominantly performed using $\text{Al}_2\text{O}_3(0001)$ substrates. There are two different stacking sequences in which TiC(111) can grow on $\text{Al}_2\text{O}_3(0001)$; this results in the formation of twin domains (see, e.g., section 7.1.3 and **Paper IX**).

A phenomenon related to epitaxy is *topotaxy*. There are a few slightly different definitions of topotaxy,⁴ but it can be defined as *conversion of a crystal into one or more products with crystal orientations that are correlated with crystal orientations in the original crystal*. Decomposition of Ti_3SiC_2 by out-diffusion of Si is an example of a topotactic reaction.⁵ **Papers VII** and **VIII** investigate this decomposition mechanism for Ti_3SiC_2 thin films.

6.3 Polycrystalline film growth

Films deposited onto amorphous substrates will generally start growing in V-W mode, i.e., island growth. The same is essentially true for polycrystalline substrates, although local epitaxial relations may come into effect. For elemental polycrystalline films, growth occurs in the following manner:⁶ after initial island formation (i.e., nucleation), the islands grow and coalesce into larger islands. During this coalescence process, there is also a strong driving force for coarsening, which means that islands with lower energy per atom consume other islands, resulting in larger crystalline islands. Coarsening occurs because the system strives to minimize its total energy. As a consequence of coarsening, many thin films exhibit preferential crystalline orientation,

[†] The terms *local* and *global* epitaxy can be used to differ between the two uses of the word *epitaxy* – but it is the same basic physical phenomenon.

even when deposited on amorphous or randomly-oriented polycrystalline substrate. Typically, the preferred orientation will be a close-packed direction, e.g., [111] for fcc metals. When the coalescence and coarsening processes have proceeded sufficiently to form a continuous film structure, the film proceeds to grow in columns. The lateral size of these columns is largely determined by the growth temperature.

The above model is developed and reasonably well understood for elemental films. Binary, ternary, and higher-order materials systems will evidently follow the same basic principles; however, effects such as relative phase stability and composition will be important. To take a relevant example, crystalline – even epitaxial – TiC_x can be grown at low temperature (100 °C).⁷ However, if the C content exceeds the stability range of TiC_x (see section 3.2), it is energetically favorable to form amorphous C in addition to crystalline TiC_x . The presence of amorphous C hinders the growth of large TiC_x crystallites. This effect is not necessarily detrimental; such approaches are employed for design of nc-TiC/a-C nanocomposites.⁸ In a ternary system, such as the Ti-Si-C system, yet another degree of freedom (a third element) is added.

6.4 Control of film growth

After understanding *how* films grow (sections 6.1 – 6.3), it is of interest to *control* film growth, and consequently the resulting microstructure. The key idea to achieve this control is to provide energy to the growing film. This can be done in many ways; some of the most important ones are that the deposited species themselves have a kinetic energy, that thermal energy can be provided by heating the substrate, and that energy can be provided by bombarding the film with energetic species; e.g. bombardment by sputtering-gas ions can be achieved by applying a bias voltage.

Understanding how the resulting microstructure can be controlled by these different means of providing energy to the growing film is the aim of developing *structure zone models* (SZM).^{6,9} Figure 6.2 shows a schematic example of a SZM, representing the microstructural evolution of elemental polycrystalline films as a function of the *homologous temperature*, defined as T_s / T_m , where T_s is the substrate temperature and T_m is the melting temperature of the material. There are three regions in this SZM. Zone I corresponds to very low deposition temperature with negligible adatom diffusion. The structure is underdense and columnar with a fine fiber texture; the columns are generally not single grains, and the orientation is random. Zone T (‘T’ for ‘transition’) corresponds to higher temperature and thus increased adatom surface diffusion, resulting in a more dense columnar structure than in zone I. The crystalline orientation is still essentially random. Zone II corresponds to high temperature, where both bulk and surface diffusion are important, resulting in dense films with large textured grains.

More complex SZMs can be developed by accounting not only for temperature, but also for the effects of ion bombardment. The classic examples are the Thornton SZMs, which appear in most textbooks.^{1,10} These were developed in the 1970s, based on relatively low-resolution optical and scanning electron microscopy observation. More refined SZMs can be developed using also transmission electron microscopy and scanning probe microscopy techniques, supported by computational studies.⁶

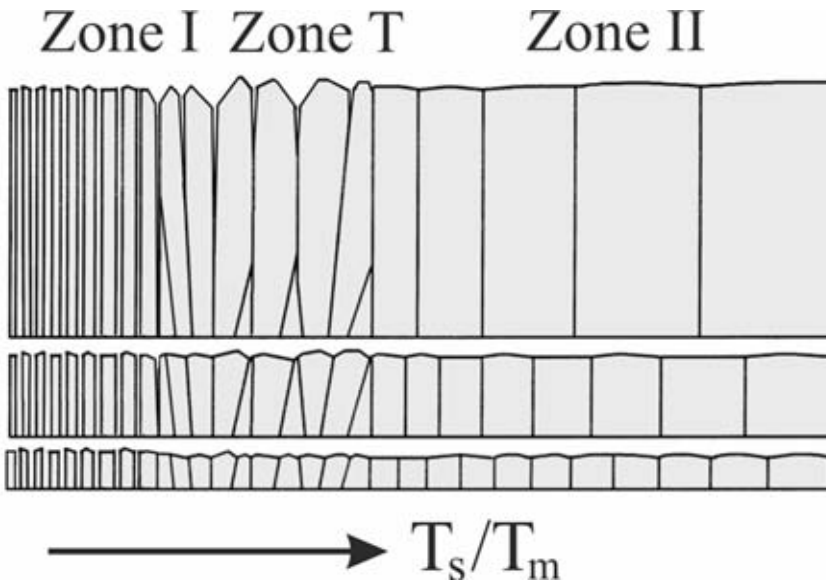


Figure 6.2 Schematic structure zone model representing microstructural evolution as a function of homologous temperature.

SZMs are useful tools; they show how parameters such as temperature and ion bombardment can be varied in order to control film growth and the resulting microstructure. However, it must also be remembered that all of the above, as well as any other, means of controlling film growth involve a trade-off, such as that between thermalized and ballistic deposition flux described in section 5.1.4; i.e., the sputtering-gas pressure and target-to-substrate distance are important parameters to select for any given requirement. Ion bombardment provides energy to the growing film but can also cause significant resputtering. Energy provided by substrate heating must be weighed against the requirement that the substrate must withstand high temperature, limiting the choice of substrates. Furthermore, an increased temperature increases the probability for desorption of adatoms. An example of the latter is the evaporation of Si observed above 900 °C in **Paper II**. This effect is a marginal issue in growth of Ti-Si-C films; however, for MAX-phase growth in systems where the A element is more volatile than Si (e.g., Ti-Al-C) A-element evaporation can be a very important effect.¹¹

-
- ¹ M. Ohring *The Materials Science of Thin Films* Academic Press, San Diego, CA (1992)
- ² D. A. Porter and K. E. Easterling *Phase transformations in metals and alloys* Taylor & Francis, Boca Raton, FL (1992)
- ³ J. Ågren *On the classification of phase transformations* Scripta Materialia 46 893 (2002)
- ⁴ R. D. Shannon and R. C. Rossi *Definition of topotaxy* Nature 202 1000 (1964)
- ⁵ M. W. Barsoum, T. El-Raghy, L. Farber, M. Amer, R. Christini, and A. Adams *The topotactic transformation of Ti_3SiC_2 into a partially ordered cubic $Ti(C_{0.67}Si_{0.06})$ phase by the diffusion of Si into molten cryolite* Journal of the Electrochemical Society 146 3919 (1999)
- ⁶ I. Petrov, P. B. Barna, L. Hultman, and J. E. Greene *Microstructural evolution during film growth* Journal of Vacuum Science and Technology 21(5) S117 (2003)
- ⁷ H. Högberg, J. Birch, M. P. Johansson, L. Hultman, and U. Jansson *Deposition of epitaxial transition metal carbide films and superlattices by simultaneous direct current metal magnetron sputtering and C_{60} evaporation* Journal of Materials Research 16 633 (2001)
- ⁸ D. Galvan, Y. T. Pei, J. Th. M. de Hosson *Reactive magnetron sputtering deposition and columnar growth of nc-TiC/a-C:H nanocomposite coatings* Journal of Vacuum Science and Technology 24 1441 (2006)
- ⁹ P. B. Barna and M. Adamik *Fundamental structure forming phenomena of polycrystalline films and the structure zone models* Thin Solid Films 317 27 (1998)
- ¹⁰ J. A. Thornton *High rate thick film growth* Annual Reviews in Materials Science 7 239 (1977)
- ¹¹ J. Frodelius, P. Eklund, M. Beckers, H. Högberg, and L. Hultman (unpublished).

7 Characterization of materials

“I see wondrous things!”

Howard Carter, 1922, upon entering the tomb of Tut-Ankh-Amun

This chapter contains brief descriptions of the materials characterization methods I have used in this work. The physics and chemistry behind each method is not the focus of the chapter, nor is the instrumentation. Instead, the central point of the chapter is the information obtained from each method. Unfortunately, materials characterization can only provide us with *information*. To turn this into *knowledge* about a material requires thinking and the ability to combine information from several different sources. How I have done that in this work is the subject of chapter 8.

7.1 Structural characterization

7.1.1 Scanning Electron Microscopy (SEM)

SEM¹ is mainly used for topographical studies where the surface of the sample is examined in three dimensions. The resolution is several orders of magnitude better than in an optical microscope, and the depth of field is larger. In terms of resolution, the SEM cannot compete with the transmission electron microscope. The SEM, however, is much simpler to use and requires little or no sample preparation. This combination of relative simplicity and good performance has made it a very common instrument in both industrial and research laboratories. The basic idea in the SEM is to scan a focused electron beam over the surface of the sample and at the same time detect the electrons emanating from every point of the surface. Any kind of interaction between the electron beam and the sample can be used to obtain contrast. The interaction has to be detected and transformed into an electric current. The most common contrast mode is secondary-electron detection, which provides a topographical image of the surface. By instead using backscattered electrons, compositional contrast can be obtained.

7.1.2 Transmission Electron Microscopy (TEM)

TEM² is a technique that allows investigation of materials down to the atomic scale; its point resolution is below 2 Å. In TEM, an electron beam is transmitted through a thin sample (< 200 nm). The interaction between the electron beam and the sample provides a means of obtaining contrast, i.e., an image of the sample. Further, it is possible to obtain crystallographic information via electron diffraction patterns, as well as chemical information through spectroscopic techniques.

The requirements on sample thickness turn sample preparation for TEM into a relatively cumbersome task. The operation of the microscope itself requires highly skilled personnel, and the instrument is expensive. These limitations makes TEM a method primarily used at universities and research institutes; compared to SEM, TEM is not common in industrial laboratories.* However, despite these drawbacks, TEM is an excellent tool for materials analysis, and gives information very difficult to obtain in any other way.

7.1.3 X-ray Diffraction (XRD)

XRD is one the most versatile techniques for structural analysis of materials.^{3,4} With XRD, it is not only possible to identify the crystalline phases in a sample; numerous structural properties can also be accurately determined: strain state, grain size, epitaxy, preferred orientation, and more. The technique is based on Bragg's law, which gives the positions of possible peaks in the X-ray diffractogram after the X-rays have scattered against a crystalline material. A standard mode of operation is called $\theta - 2\theta$ scans. Here, the incident beam and the detector are scanned synchronously over the angular range. The incident angle is θ and the angle between the incident beam and the detector is 2θ , hence the name $\theta - 2\theta$ scan. The thus detected peaks in the diffractogram are used to identify the crystalline phases present in the sample.

For nanocrystalline materials, the grain size is an important parameter, which can be determined from the peak broadening of the corresponding XRD peak. The full width at half of the maximum intensity (FWHM) is correlated to the grain size.

It is often interesting, especially in thin film work, to determine the preferred orientation, or *texture*, of a sample. There are several forms of texture: random orientation (i.e., no texture), fiber texture, where the in-plane orientation is random but there is a preferred out-of-plane orientation, biaxial texture, where there is an in-plane mirror symmetry, and epitaxy (see section 6.2), where all in-plane and out-of-plane orientations are unique. Texture can be investigated by X-ray diffraction *pole figures*. This means that the Bragg angle of a specific reflection (originating from a specific set of lattice planes) is chosen, i.e., the 2θ angle is fixed. Then, the azimuth angle ϕ and the tilt angle ψ are scanned, measuring the intensity of the reflections from these lattice planes in all possible directions. An example (from **Paper IX**) can be seen in Figure 7.1, which is a pole-figure plot of the TiC 111 peak from an epitaxial TiC/SiC multilayer. A predominant 111 peak can be seen at zero ψ and ϕ , with six additional peaks at $\psi \approx 70.5^\circ$, due to the threefold symmetry of $\{111\}$ planes and twin-domain formation in the TiC layer. TiC twin-domains are formed since there are two different stacking sequences in which TiC(111) can grow on $\text{Al}_2\text{O}_3(0001)$.

7.1.4 Atomic Force Microscopy (AFM)

The AFM technique¹ belongs to a family of techniques referred to as Scanning Probe Microscopes (SPM). It uses a sharp tip mounted on a flexible cantilever. When the tip comes to within a few ångströms of the surface of the sample, the repulsive van der Waals forces deflect the cantilever. This deflection is converted into a current. When the cantilever is scanned over a surface, an image of the surface is obtained. AFM is

* That does not mean that industry does not use TEM at all – just that there are relatively few companies that have their own TEMs, and that TEM is not a routinely used technique, unlike SEM and optical microscopy.

particularly suitable when additional information, other than just the image, is desired. One important such example is the surface roughness, which can readily be calculated from the obtained image.

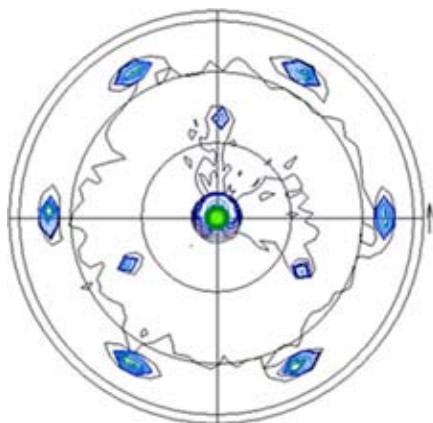


Figure 7.1 XRD pole-figure plot of the TiC 111 peak for an epitaxial TiC/SiC multilayer with SiC-layer thickness of 1 nm. From Paper IX.

7.2 Compositional characterization

7.2.1 X-ray Photoelectron Spectroscopy (XPS)

X-ray Photoelectron Spectroscopy¹ (XPS) is also known as Electron Spectroscopy for Chemical Analysis (ESCA). While the former, more commonly used, acronym emphasizes the physics behind the technique, the latter concentrates on the applications of the method. The sample is irradiated with X-ray photons of a known energy, $h\nu$. If this energy is high enough, electrons will leave the atoms in the sample with a kinetic energy (E_{kin}) equal to $h\nu$ minus the binding energy, E_B . The kinetic energy is measured and the intensity is plotted against E_B . Since the binding energy specific to each element is known, this can be used to identify the elements in the sample. In XPS, a standard X-ray tube such as AlK α is normally used. Another option is to use synchrotron radiation (**Paper VII**), where the energy of the incoming photons (and, correspondingly, the surface sensitivity) can be varied in a large range.

An important feature of XPS originates from the fact that it probes the core electron levels. These are not affected largely by the surrounding atoms. Nevertheless, there will be a small shift in E_B , known as a *chemical shift*, due to the influence of neighboring atoms. This permits determination of the types of chemical bonds present in a material.

In order to perform an accurate quantitative chemical analysis with XPS, a standard sample of known concentration is required. From the peak area measured with this

standard sample, *sensitivity factors* S_i , are determined. For example, the Ti concentration in a Ti-Si-C sample is then given by

$$c_{Ti} = \frac{A_{Ti} / S_{Ti}}{A_{Ti} / S_{Ti} + A_{Si} / S_{Si} + A_c / S_c}, \quad (7.1)$$

where A_i are the peak areas of element i . In this work, a Ti_3SiC_2 sample was used to determine the sensitivity factors. The accuracy of the sensitivity factors was verified with a $TiC_{0.66}$ sample; XPS gives a value of the C/Ti ratio of 0.66 ± 0.02 . It should be mentioned that for the nc-TiC/a-SiC samples studied in, e.g., **Paper III**, the accuracy for Si may be somewhat less good, since the bonding is different in the standard sample and in nc-TiC/a-SiC. In Ti_3SiC_2 , the Si bonds to Si, while the nc-TiC/a-SiC samples predominantly exhibit Si-C bonding.

With XPS, it is possible to obtain a depth profile of a sample using sputtering with, e.g., Ar gas. This is frequently necessary, since XPS is a surface sensitive technique; the majority of the signal comes from the top 10 – 40 Å of the sample. For example, this means that information on surface oxides and adsorbed hydrocarbons can be obtained. However, this does not give accurate information on the actual composition of the sample; consequently, a depth profile must be acquired (see, however, section 9.1). It is important to understand that depth profiling by sputtering is a destructive process and may affect the composition of the sample, since different elements have different sputtering yields. This underlines the necessity of using standards of known composition to obtain reliable quantitative data.

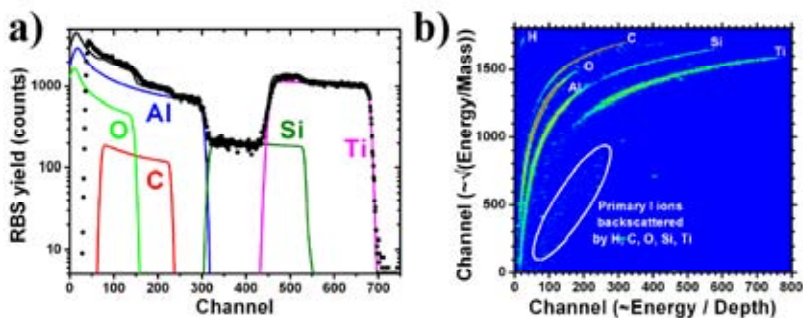


Figure 7.2 (a) Spectrum from RBS measurement, where the circles are measured data points and the solid curves are the results of a least-square fit, and (b) ERDA contour plot.

7.2.2 Energy-dispersive X-ray Spectroscopy (EDX or EDS)

An electron microscope is not limited to imaging: the possibility of combining an electron microscope (SEM or TEM) with an Electron Probe Microanalyzer (EPMA) provides a powerful tool for chemical analysis.¹ The EPMA analyses the characteristic X-ray photons emitted from the elements in the sample, i.e., the “fingerprints” of the elements. There are two types of EPMA: Wavelength Dispersive X-ray Spectroscopy (WDX/WDS) and Energy Dispersive X-ray Spectroscopy (EDX/EDS). The lat-

ter is much faster and therefore the more widespread of the two. However, WDX has a significantly better resolution, and its accuracy is superior to that of EDX. The great advantage of EDX is that a qualitative determination of the elements present in a sample is rapidly performed. Additionally, it is possible to obtain information on the distribution of elements over the examined area by mapping. Quantitative analysis requires reference spectra from a sample with a known composition. While qualitative and semi-quantitative measurements are rapidly performed with EDX, accurate quantitative analysis is, in many cases, quite difficult and must be performed with great care and expertise (which is not always the case in the literature). Further, it is not possible (like in XPS) to obtain the type of bond or chemical shifts. Another important disadvantage of EDX is that light elements, such as C, are notoriously difficult to quantify. This latter feature makes EDX a technique with limited applicability to my work; however, I use it for *qualitative* measurements. Examples are the line scans used in **Papers II** and **VIII** to investigate variations in composition.

7.2.3 Ion-beam analysis

Elastic Recoil Detection Analysis (ERDA or just ERD) and its close relative Rutherford Backscattering Spectrometry (RBS) are ion-beam techniques used for compositional analysis in materials science.⁵

In RBS, a high-energy (several MeV) ion beam with low-mass ions, usually He (sometimes H), is used. The ion beam irradiates the sample at normal incidence angle. The incident ions are backscattered from the sample with energies that depend on both the atomic mass of the atoms by which they are backscattered, and the distance (depth) at which each scattering event occurs. The information obtained is therefore a combination of composition and depth, and is shown as a plot of the number of backscattered ions as a function of the energy of the backscattered ions (or “counts” vs. “channel number”, which is essentially the same). Such a plot is shown in Figure 7.2(a). Subsequently, a least-square fit to the obtained curve enables determination of the compositional depth profile (with a depth resolution of ~10 nm) of the sample.

RBS has many important advantages: it is a standardless method (i.e., does not require standard samples like XPS and EDX do), relatively quick, normally nondestructive, and can be used for depth profiling. However, RBS has one serious flaw – although it can detect light elements, it is inaccurate due to the low backscattering yield. Since a very important aspect of the compositional analysis in my work is to accurately determine the C content in Ti-Si-C thin films, ERDA is a more suitable option.

In ERDA, just like in RBS, the sample is irradiated by a high-energy ion beam, but the ions are heavier. Typically, iodine or chlorine ions with energies of several tens of MeV are used. Additionally, the angle of incidence is not normal, but typically 15 - 25°. This results in a combination of several outgoing species. For example, I ions incident on a sample consisting of a Ti-Si-C thin film on an Al₂O₃ substrate (as in **Paper II**) will yield not only backscattered I ions, but also elastically recoiled[†] Ti, Si, C, Al, and O ions with energies that depend on both the atomic mass of the respective atom and the depth at which each recoil event takes place. At the detector, there is a mass separation filter followed by an energy spectrometer. The information obtained is therefore a complex combination of mass, composition and depth, and is shown as a

[†] The term “forward-sputtered” is often used as a synonym for “elastically recoiled” in this context.⁵

contour plot. Figure 7.2(b) is an example of such a contour plot. The different branches observed in the contour plot correspond to the individual masses of the recoiled species. The projection of each branch on the x-axis is therefore essentially the same “counts” vs. “channel number” plot as obtained in RBS, and can be analyzed in the same manner to obtain a compositional depth profile.

For my work, it is important that ERDA has all the advantages of RBS mentioned above, but with the additional possibility to relatively accurately determine the C content (as well as any O, N, and H impurities). This is not possible or at least very difficult with EDX, and ERDA does not have the requirement of XPS for reliable standard samples. Unlike XPS, however, ERDA cannot determine chemical shifts.

7.3 Electrical characterization

7.3.1 Resistivity

A common way to measure the resistivity of a thin film is the four-point-probe technique.⁶ Four equidistant probes are pressed against the film (Figure 7.3 (a)), two measuring the current through the film, and two measuring the corresponding voltage drop. The measured value is called the *sheet resistance* and is defined as $R_s = \rho / d$, where ρ is the specific resistivity (in Ωm , or $\mu\Omega\text{cm}$) and d is the film thickness. An important feature of the technique is that R_s (in the unit Ω/square and with the dimension of resistance) is independent of the distance between the probes. The resistivity can be determined from the measured value of R_s by multiplying with the film thickness (which must be determined independently).

For films exhibiting metallic behavior, Matthiessen’s rule applies. As seen in Figure 7.3(b), the total resistivity is the sum of the contributing individual resistivities, which arise due to thermal electron scattering as well as scattering at defects and impurities.

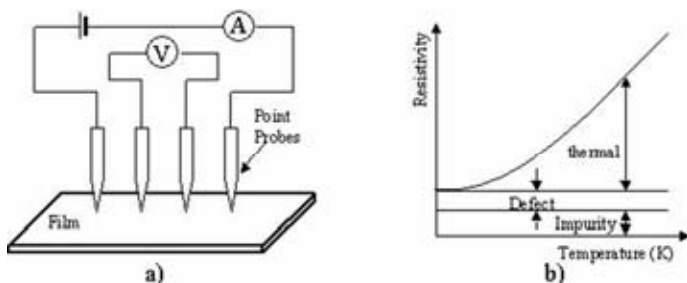


Figure 7.3 (a) Schematic of the four-point probe measurement setup, and (b) contributions to the measured resistivity.

7.3.2 Electrical contacts

Electrical contacts are an application of particular interest to the research and industrialization project that inspired (and funded!) my Thesis work. **Paper III** deals with the use of Ti-Si-C coatings in electrical-contact applications.

In his classic textbook,⁷ Holm^{‡,§} defined the term *electric contact* as a “releasable junction between two conductors which is apt to carry electric current”.[§] Electrical contacts can be divided into *stationary*, *sliding*, *switching*, and *rolling* contacts. They are found in *all* electrical systems, from consumer appliances and office computers to heavy industry and power transmission, and are therefore of vast technological and economical importance. The performance of electrical contacts depends on the contact materials. While any electrical contact must be optimised for a particular application, there are several generally desired properties for electrical-contact materials.^{9,10} Apart from being inexpensive and environmentally benign, contact materials should be electrically and thermally conducting and be corrosion resistant. They should be ductile, welding resistant, and for non-static contacts, wear-resistant and exhibit low friction. Dominant electrical-contact materials are noble metals like Au or Ag, since they are conductive, ductile, and corrosion-resistant. However, they frequently exhibit problems with welding, wear, and friction. Additionally, Au is expensive and Au mining is environmentally problematic, due to the use of cyanide. To address these issues, the electrical-contact industry has shown considerable interest in conducting ceramics and metal/ceramic composites.

The term *contact resistance* refers to the measured voltage drop over the contact divided by the current, and is the figure of merit for any electrical contact. The requirements are that the contact resistance be low and, more importantly, stable over the lifetime of the application.¹⁰ It is important to remember that contact resistance is not an intrinsic property of a material but depends on application, contamination, sample history, etc.

In the field of electrical contacts, the term *coating* (or *finish*) is used, rather than *thin film*, to describe a material deliberately applied to a substrate. The term *film* is by convention used for contaminants and passivating films. PVD techniques like sputtering are not widespread in the electrical-contact industry. Electroplating is the dominating coating method,⁹ while PVD processing is often perceived as expensive and slow. This may have been true in the past, but modern industrial sputtering systems are in general fully competitive with electroplating in terms of cost and throughput, and superior in terms of coating quality. Furthermore, PVD has a major advantage over electroplating in that the latter is severely limited when it comes to choice of material; electroplating is restricted to some metals and metal alloys.

[‡] Ragnar Holm (1879-1970), Swedish scientist, also active in Germany and the US. He is considered the father of modern electrical-contact theory. He was honored by IEEE in that the annual IEEE Conference on Electrical Contacts is called the “Holm Conference”.

[§] Note the important word “releasable” in Holm’s definition. This does not cover, e.g., Ohmic and Schottky contacts to a semiconductor – a difference in terminology between the fields of semiconductor devices and electrical contacts; the term *contact resistance* also carries a somewhat different meaning. This nomenclatural difference can cause considerable confusion.

7.4 Mechanical characterization

7.4.1 Nanoindentation

One of the most well suited techniques for mechanical characterization of nanostructured materials is called nanoindentation. The method permits determination of hardness and elastic modulus (Young's modulus). In a nanoindentation measurement, an indenter is pressed into the surface of a material while the applied force and the displacement of the indenter are recorded. From the load-displacement curve (Figure 7.4), the hardness and the reduced elastic modulus can be found according to the Oliver-Pharr method.¹¹ The reduced elastic modulus, E_r , is defined as

$$\frac{1}{E_r} = \frac{(1-\nu^2)}{E} + \frac{(1-\nu_i^2)}{E_i}, \quad (7.2)$$

where E_i is the elastic modulus of the indenter (1141 GPa for diamond), ν and ν_i are Poisson's ratio for the material under test and the indenter, respectively, and E is the real elastic modulus.

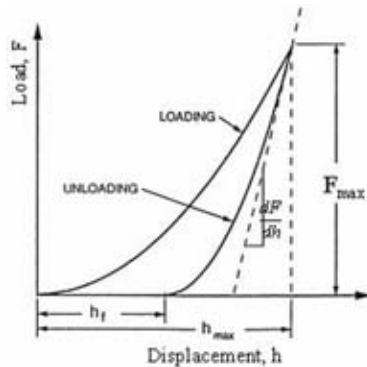


Figure 7.4 Schematic of the load-displacement curve recorded during a nanoindentation measurement.

The response of a material to indentation depends on its mechanical characteristics. Ceramic materials, typically brittle and hard, tend to exhibit sink-in behavior, while materials that are more ductile (e.g., metals) instead exhibit pile-up around the indent. These effects are shown in Figure 7.5. The nanoindenter I have used is connected *in situ* to an AFM, permitting imaging of the indents and direct observation of whether pile-up or sink-in has occurred.

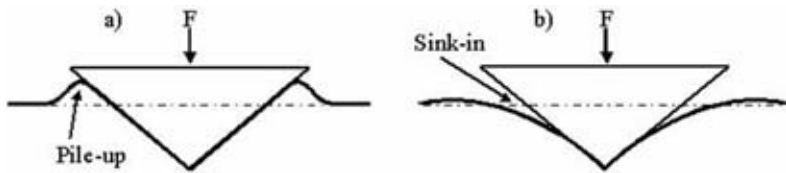


Figure 7.5 a) The pile-up behavior typical of ductile materials such as metals, and b) the sink-in behavior typically exhibited by hard and brittle materials like ceramics.

¹ C. R. Brundle, C. A. Evans Jr., and S. Wilson *Encyclopedia of Materials Characterization* Butterworth-Heinemann, Boston, MA (1992)

² D. B. Williams and C. B. Carter *Transmission Electron Microscopy* Plenum Press, New York (1996)

³ B. D. Cullity *Elements of X-Ray Diffraction* 2nd ed. Addison-Wesley, Reading, MA (1978)

⁴ M. Birkholtz *Thin Film Analysis by X-ray Scattering* Wiley-WCH, Weinheim, Germany (2006)

⁵ J. R. Tesmer and M. Nastasi (ed.) *Handbook of modern ion beam analysis* Materials Research Society, Pittsburgh, PA (1995)

⁶ M. Ohring *The Materials Science of Thin Films* Academic Press, San Diego, CA (1992)

⁷ R. Holm, *Electric Contacts, Theory and Application*, 4th ed., Springer-Verlag, Berlin (1967)

⁸ T. Kaiserfeld Ragnar Holm and *Electric Contacts: A Career Biography in the Shadow of Industrial Interests* Proceeding of the 20th International Conference on Electrical Contacts, Stockholm, Sweden 13 (2000)

⁹ W. Rieder *Electrical Contacts: An Introduction to their Physics and Applications* IEEE, Piscataway, NJ, 2005

¹⁰ P. G. Slade (ed.) *Electrical Contacts-Principles and Applications* Marcel Dekker, New York, 1999

¹¹ W. C. Oliver and G. M. Pharr *An improved technique for determining hardness and elastic modulus using load and displacement sensing indentation experiments* Journal of Materials Research 7 1564 (1992)

8 Summary and contribution to the field

“I’d like to have an argument, please.”

Man (Michael Palin), in Monty Python’s “Argument Clinic”

This chapter is a summary of the papers included in this Thesis, and a discussion on how my work may contribute to the research field.

8.1 MAX-phase thin-film growth

Investigation of sputtering-synthesis of MAX-phases in the Ti-Si-C system began with Seppänen *et al.*,¹ Palmquist *et al.*,^{2,3} and Emmerlich *et al.*.⁴ In their work, the emphasis was on sputtering using elemental sources, i.e., three separate Ti, Si, and C targets, and model substrates such as MgO and Al₂O₃. This setup is well-suited for fundamental research on growth and properties of MAX phases, due to the individual control of the elemental fluxes and the well-defined substrate surfaces. **Paper I** expands these studies by addressing growth of thin-film Ti₃SiC₂ on bulk Ti₃SiC₂ substrates. I show that the crystallographic orientation of the film grains is determined by the respective substrate-grain orientation, i.e., homoepitaxial MAX-phase growth can be obtained. A parallel can be drawn with the TiC(111) seed layer used in other work² to provide a crystallographic template for epitaxial Ti₃SiC₂ growth. The Ti₃SiC₂ {0001} and TiC {111} planes can form epitaxial and coherent interfaces. This follows from the isomorphism of the TiC(111) and the Ti₃SiC₂(0001) low-energy surfaces and the corresponding strong tendency for basal-plane-oriented growth of Ti₃SiC₂ on TiC{111} planes. The growth orientation of the MAX-phase film is therefore governed by the orientation of the substrate grain, upon which it is grown, i.e., tilted basal-plane growth following the MAX-phase substrate-grain orientation. Low Si content results in growth of TiC with Ti₃SiC₂ as a minority phase. For higher Si content, the films predominantly consist of MAX phases, both Ti₃SiC₂ and the metastable Ti₄SiC₃, while excess Si is a limiting factor for Ti₃SiC₂ growth. In other words, there is a growth window in which thin-film Ti₃SiC₂ can be grown homoepitaxially on bulk Ti₃SiC₂.

As said above, the use of elemental sources is suitable for fundamental studies. For applied studies and especially for potential industrial processes, however, use of compound targets is generally preferred for reasons of simplicity and repeatability. The groundbreaking studies of Seppänen *et al.*¹ and Palmquist *et al.*² demonstrated synthesis of Ti₃SiC₂(0001) thin films on MgO(111) using a Ti₃SiC₂ compound target with a TiC_x(111) seed layer. There are, however, several unresolved issues with sputtering from a compound target, such as the phase purity and the film composition, which

may be quite different from that of the target. **Paper II** addresses Ti-Si-C MAX-phase growth from a Ti_3SiC_2 target (see also section 8.3). As-deposited films exhibit a significant amount of excess C compared to the target composition, preventing MAX-phase growth. Addition of Ti (sputtered from a separate target) throughout the process was employed to compensate for the excess C, providing a means of synthesizing phase-mixed films of TiC_x , Ti_3SiC_2 , and Ti_4SiC_3 . A large amount of added Ti, on the other hand, resulted in growth of films consisting mainly of (111)-oriented TiC_x . Further, such TiC_x films were employed as a buffer layer for MAX-phase synthesis. This is a parallel to the work of Palmquist *et al.*,² where it was shown that a $\text{TiC}_x(111)$ seed layer was required to promote growth of epitaxial Ti_3SiC_2 when deposited from a Ti_3SiC_2 target; however, with lower purity than Ti_3SiC_2 synthesized from elemental targets (where a seed layer is not required). My results provide an explanation for why a seed layer is important to achieve Ti_3SiC_2 growth from a compound target. Not only does a $\text{TiC}_x(111)$ seed layer provide a crystallographic template upon which Ti_3SiC_2 can grow; the seed layer can also accommodate the excess C, which can diffuse into the buffer layer. This results in a composition of the growing film relatively close to the correct composition to form Ti_3SiC_2 . After some time, however, this buffering effect expires, and the MAX-phase growth is again hindered by the excess C which no longer can diffuse into the TiC_x layer since the required diffusion length scale is too long, and the TiC_x has become saturated in C.

8.2 Low-temperature deposition and electrical properties of Ti-Si-C-based nanocomposite thin films

An important issue for industrial application of thin-film MAX phases such as Ti_3SiC_2 is the substrate temperature. As discussed in section 3.5.2, the substrate temperature required for MAX-phase formation is typically 700 – 1000 °C. Even the 450 °C demonstrated for V_2GeC and Cr_2AlC (see section 3.5.2) is not sufficiently low to permit deposition on a wide range of common metal substrates (e.g., Cu or Al) with respect to their thermal and structural stability. Although there are some relevant substrate-materials that withstand 450 – 500 °C (e.g., some steels), temperatures below 300 °C (preferably even lower) are required for general applicability to deposition on metals. Ti-Si-C deposition at low temperature is a main theme of **Papers III** and **IV**.

In **Paper III**, Ti-Si-C thin films were produced using magnetron sputtering from a Ti_3SiC_2 target at 300 °C. The as-deposited films were found to be nanocomposites comprising TiC nanocrystallites embedded in an amorphous SiC matrix (nc-TiC/a-SiC). Such nanocomposites have previously been investigated by several authors dealing with mechanical properties for potential applications as hard coatings, but only very limited investigations of *electrical* properties have been performed. The nc-TiC/a-SiC nanocomposites were employed as electrical-contact material. When contacted against Ag, they exhibit somewhat higher contact resistance than Ag against Ag, while preventing welding, an otherwise serious problem in noble-metal contacts. This is due to an adequate resistivity ($\sim 300 \mu\Omega\text{cm}$) coupled with beneficial mechanical properties, exemplified by relatively high nanoindentation hardness of 20 GPa, but a ductile deformation behavior that results in a large contact area. The ductility can be explained by rotation and gliding of nc-TiC grains in the matrix. In summary, the *combination* of electrical and mechanical properties allows the use of nc-TiC/a-SiC nanocomposites as a *multifunctional* coating material in electrical-contact applications.

Many electrical applications, however, require a considerably lower resistivity than the $\sim 300 \mu\Omega\text{cm}$ of the nc-TiC/a-SiC. This issue can be addressed by alloying with a highly conductive noble metal. In **Paper IV**, the effect of Ag addition to Ti-Si-C coatings on microstructure and electrical resistivity was investigated. As a consequence of the strong segregation tendencies in the system, a structure comprising nanocrystalline TiC and Ag in an amorphous Si-based matrix is formed. The resistivity could indeed be decreased by a factor of 2 – 10 (dependent on Ag content) compared to Ti-Si-C thin films without Ag. For high Ag content, a large decrease in resistivity is expected given the large volume fraction of the very good conductor Ag. For low Ag content, however, no significant change in resistivity is expected if only Ag is responsible for the improved conductivity compared to Ti-Si-C thin films without Ag. Thus, a more complex model involving conduction paths through Ag, TiC_x, and/or the matrix is required to explain the resistivity at low Ag content. A possibility is if a part of the Ag forms a highly conductive tissue phase; another possibility is that a small amount of Ag is dissolved in the Si matrix thus greatly decreasing its resistivity. However, determination of whether an Ag tissue phase is present or not is very challenging both in terms of sample preparation and electron-microscopy analysis, and more work is required to understand electrical-conduction mechanisms in Ti-Si-C-Ag nanocomposites.

8.3 Compound-target sputtering processes

Papers II and **V** (to some extent also **Papers III** and **IV**), address the complex issue of understanding the sputtering process from a Ti₃SiC₂ target.

For MAX-phase growth from a Ti₃SiC₂ target (**Paper II**), it is essential to understand the process and what causes the compositional differences between the film and the target. This understanding is necessary since growth of MAX phases requires stoichiometric conditions due to the very limited MAX-phase stability ranges.

As discussed in **Paper II**, a number of possible causes for the difference between the film composition and the target composition can be suggested. Some can easily be ruled out or deemed unlikely, for example different sticking coefficient of the species (since there is temperature dependence), resputtering by Ar ions in the plasma (since there is no applied bias) or resputtering by Ar neutrals backscattered from the target (since the amount of backscattered Ar neutrals is small). It cannot completely be ruled out that the outgoing flux from the target is different from the nominal composition. This may occur due to in-diffusion of C into the racetrack region of the target during deposition as target heating is unavoidable. This is, however, not supported by XPS composition determination of the racetrack of a used target, which showed no excess C. Instead, the compositional differences between the film and the target are likely mainly due to the angular and energy dependence of the sputtered flux and gas-phase scattering processes during the transport phase.

Paper V presents a study of high-power impulse magnetron sputtering (HIPIMS) growth of Ti-Si-C films from a Ti₃SiC₂ compound target. An important difference between HIPIMS and dc magnetron sputtering is the high degree of ionization obtained in HIPIMS (see section 5.2.2). For deposition from a compound target, the degree of ionization is a particularly important parameter as it differs between elements (e.g., a few percent for C and up to 90 % for Ti). This means that the film structure

and composition can be controlled to some extent by an appropriate choice of process parameters such as pressure, substrate inclination angle, and bias. Furthermore, the compositional variations for films deposited on inclined substrates at different pressures show that the C content is strongly affected by gas-phase scattering, in parallel to the results in **Paper II**. Given the fact that the degrees of ionization of Ti and Si are much higher than that of C, Ti and Si are to a much larger extent than C attracted to the biased substrate.

8.4 Properties of MAX phases and nanocomposites

8.4.1 Electrical properties of MAX phases

Paper VI deals with the effect on electrical properties of substitution of the A element in Ti-A-C MAX phases, specifically Ti_3SiC_2 , Ti_4SiC_3 , Ti_3GeC_2 , Ti_2GeC , and Ti_2SnC . The resistivity values measured for the thin films show that they are good conductors and exhibit resistivity values of: $\sim 21 - 51 \mu\Omega\text{cm}$ for Ti-Si-C films, $\sim 15 - 50 \mu\Omega\text{cm}$ in the Ti-Ge-C system, and $\sim 46 \mu\Omega\text{cm}$ for Ti_2SnC . A general trend of increased resistivity with higher n is observed: $21-32 \mu\Omega\text{cm}$ for Ti_3SiC_2 films, $\sim 50 \mu\Omega\text{cm}$ for Ti_4SiC_3 . Ti_2GeC thin films exhibit resistivity values as low as $15 \mu\Omega\text{cm}$, while Ti_3GeC_2 and Ti_4SiC_3 show higher values of $\sim 50 \mu\Omega\text{cm}$. These results are in accordance with the conduction mechanism of MAX-phases, and can be attributed to the presence of A-element layers that weaken the Ti(1)-C bonds thereby enhancing the strength of the metallic Ti(1)-Ti(1) bonds within the basal planes. Consequently, a material with a stronger metallic character and hence a higher conductivity than TiC is obtained.

The measured resistivity values are, however, affected by differences in crystalline quality, microstructure, composition, and impurity phases. The application of TiC_x transition or seed layers at the substrate-film interface has only a marginal effect on the measured resistivity values, but intergrown TiC_x layers in the center of a Ti_3SiC_2 film, constricts the current flow. In the Ti-Ge-C system, local surface segregation of Ge and $\text{Ti}_5\text{Ge}_3\text{C}_x$ has little effect. The resistivity in the Ti-Sn-C system is mainly affected by the segregation of metallic Sn yielding a wide spread in the measured values ranging from $20-46 \mu\Omega\text{cm}$. The lower resistivity values of $\sim 20 \mu\Omega\text{cm}$ correspond to films with pronounced segregation of Sn compared with the $\sim 46 \mu\Omega\text{cm}$ obtained for more phase-pure films.

8.4.2 Mechanical properties of nanocomposites and MAX phases

It is interesting that some mechanical properties of nc-TiC/a-SiC nanocomposite (**Paper III**) and Ti_3SiC_2 thin films^{3,5} are similar, despite the very different nature of the two types of materials. The hardness and elastic-modulus values are relatively close to each other, and both materials exhibit a ductile behavior. This ductile behavior is noteworthy as a little-explored property of related nanocomposites such as those in the nc-TiC/a-C and nc-TiN/a-Si₃N₄ systems used for superhard coatings. The ductile mechanical properties of nc-TiC/a-SiC are actually more similar to those of Ti_3SiC_2 , which is very ductile due to kinking and delamination, than those of TiC. The ductility in the nc-TiC/a-SiC nanocomposite can be attributed to rotation and gliding of nc-TiC in the matrix. Thus, nc-TiC/a-SiC and Ti_3SiC_2 are both ductile, but the deformation mechanisms are different.

The observed ductility of nc-TiC/a-SiC has a relevant parallel in the field of superhard nanocomposite coatings. Much work in that area has been directed towards achieving superhardness in coatings. In recent years, however, it has become clear that superhardness alone is not very useful – it must be combined with other properties, especially toughness (i.e., resistance to fracture and cracking).⁶ A problem is that, although there are several methods to measure toughness, no standard widely accepted method of consistent quantitative toughness determination exists (unlike hardness, where nanoindentation is ubiquitous).⁷ Nevertheless, the absence of cracking upon indentation indicates that the nanocomposite nc-TiC/a-SiC is satisfactorily tough (**Paper III**).

8.4.3 Thermal stability

Papers VII and VIII investigate the thermal stability of $\text{Ti}_3\text{SiC}_2(0001)$ thin films by *in-situ* photoemission (**Paper VII**) and XRD (**Paper VIII**) studies during annealing. The films were found to be effectively stable for annealing up to 1000 – 1100 °C. Annealing at higher temperature resulted in decomposition of Ti_3SiC_2 by Si out-diffusion to the free surface with subsequent evaporation; surface Si was directly observed by photoemission. In Ti_3SiC_2 , the Ti_3C_2 layers between Si sheets in Ti_3SiC_2 represent TiC(111) planes. The Ti_3C_2 layers are twinned to each other separated by the Si layer acting as a mirror plane. De-twinning to TiC occurs upon removal of the Si plane and rotation of the Ti_3C_2 layer, which means that, at a temperature of ~1000 °C, Si starts to diffuse out along the basal planes of the Ti_3SiC_2 structure, followed by rotation of the Ti_3C_2 structural units to form TiC. Finally, (111)-oriented TiC_x layers recrystallize at temperatures above 1200 °C.

The actual temperatures are considerably lower than the temperature required for decomposition of bulk Ti_3SiC_2 , which is effectively thermally stable up to at least 1700 °C. There is thus an apparent difference between epitaxial thin-film samples and bulk samples with respect to decomposition of Ti_3SiC_2 . There are two reasons for this. First, the diffusion length scales and the sensitivity of the analysis methods are different in the actual studies. With the high surface sensitivity (a few nanometers) of the photoemission technique (**Paper VII**) it is not surprising that the onset temperature for MAX-phase decomposition could be found. Second, with the presence of an interface to ambient (vacuum in **Papers VII and VIII**) the chemical potentials for the elements are different from the bulk situation. In the presence of oxygen, surface oxides will thus form that can act as diffusion barriers against further decomposition. The UHV conditions in **Paper VII**, presented effectively no oxidizing environment. Instead, Si - as a relatively weakly bonded atom and the fastest diffusing species compared to Ti and C - tended to segregate to the surface at 1000 °C.

Annealing of nc-TiC/a-SiC films (**Paper VII**) resulted in surface segregation of free C and to some extent also Si due to out-diffusion of both C and Si predominantly from the amorphous phase. This is in contrast to Ti_3SiC_2 , where decomposition occurs virtually exclusively by out-diffusion of Si while C remains tightly bonded in the Ti_6C octahedral structural units.

8.5 Multilayer structures

Papers IX and X investigate multilayers. The main research theme is to employ multilayers as model systems for more complex structures, e.g., nanocomposites and

MAX phases. Multilayers are useful as two-dimensional (2D) model systems of three-dimensional (3D) materials and structures. This is because multilayers permit design and investigation by, e.g., TEM, of interfaces not readily accessible in 3D.

8.5.1 Epitaxial TiC/SiC multilayers

Paper IX investigates epitaxial TiC/SiC multilayers synthesized at ~ 550 °C. With epitaxial TiC as template, the metastable 3C-SiC (normally requiring much higher synthesis temperature) is stabilized most likely due to pseudomorphic forces resulting in a retained local epitaxy. As observed for thicker SiC layers, there is a critical thickness of at least ~ 2 nm beyond which the epitaxy of the SiC layer is lost. The lattice mismatch between TiC and 3C-SiC is very small, $< 1\%$. Nevertheless, the interfacial strain increases linearly with SiC-layer thickness and after the critical thickness, energy minimization results in loss of coherent-layer growth and the formation of a-SiC. These results are relevant to the design of nanocomposite materials. As stated in section 8.2, **Paper III** demonstrated a thin-film nc-TiC/a-SiC nanocomposite material. However, determining the exact nature of the interfaces between TiC nanocrystallites and the SiC tissue phase, as well as the structure of the latter, is an extreme challenge for analytical TEM and sample preparation. In a multilayer, on the other hand, the interfaces can be isolated and probed. The multilayer study indicates that the possibility to have a *crystalline* rather than *amorphous* tissue phase in a nanocomposite must be taken into account. This may provide higher interfacial bond strength while retaining the ability to hinder dislocation gliding and grain boundary sliding. This adds a potentially important design opportunity for nanocomposite materials.

8.5.2 Epitaxial TiC/Ti₃SiC₂ multilayers

As said in section 3.3, Ti₃SiC₂ is very ductile due to kinking and delamination. Kink-band formation is the dominant deformation mechanism in Ti₃SiC₂. The actual formation of kinks is generally associated with interlaminar fracture due to the weak bonds between the atomic sheets of the structure. However, it is not clear whether the kink-band formation is the dominant deformation mechanism due to the dislocation mobility or due to the ease of interlaminar fracture. To investigate this, **Paper X** studies the deformation of Ti₃SiC₂ when interlaminar fracture is inhibited. This is achieved by separating areas of Ti₃SiC₂ with less ductile layers of another material in a laminated structure; specifically, epitaxial Ti₃SiC₂(0001)/TiC_{0.67}(111) nanolaminated multilayer thin films.

Nanoindentation showed that kink-band formation and the corresponding pile-up are inhibited in the Ti₃SiC₂/TiC_{0.67} nanolaminate, apparently as a consequence of the lamination with the less ductile TiC apparently hindered this mechanism. The hardness and Young's modulus were determined to ~ 15 GPa and ~ 240 GPa, in the range of monolithic Ti₃SiC₂. Therefore, it is interesting that even when the dominant deformation mechanism is inhibited, there is no detectable change in the apparent hardness and Young's modulus. However, in the Ti₃SiC₂/TiC_{0.67} nanolaminate the deformation of Ti₃SiC₂ is still dominated by basal-plane slip, as in monolithic Ti₃SiC₂. This remarkable response to indentation is based on persistent slip in the TiC layers and that gross slip throughout the nanolaminate was inhibited by the interleaving Ti₃SiC₂ layers. Thus, the studied Ti₃SiC₂/TiC_{0.67} model system shows that one type of layer in a nanolaminate can affect the deformation mechanism of the other on the nanometer scale.

-
- ¹ T. Seppänen, J.-P. Palmquist, P.O.Å. Persson, J. Emmerlich, J. Molina, J. Birch, U. Jansson, P. Isberg, and L. Hultman *Structural characterization of epitaxial Ti₃SiC₂ thin films* Proceedings of the 53rd Annual Meeting of the Scandinavian Society for Electron Microscopy 142 (2002) (Ed. J. Keränen and K. Sillanpää, Tampere University, Finland, ISSN 1455-4518)
- ² J. -P. Palmquist, U. Jansson, T. Seppänen, P. O. Å. Persson, J. Birch, L. Hultman, and P. Isberg *Magnetron sputtered epitaxial single-phase Ti₃SiC₂ thin films* Applied Physics Letters 81 835 (2002)
- ³ J. -P. Palmquist, S. Li, P. O. Å. Persson, J. Emmerlich, O. Wilhelmsson, H. Högberg, M. I. Katsnelson, B. Johansson, R. Ahuja, O. Eriksson, L. Hultman, and U. Jansson *M_{n+1}AX_n phases in the Ti-Si-C system studied by thin-film synthesis and ab initio calculations* Physical Review B 70 165401 (2004)
- ⁴ J. Emmerlich, J. -P. Palmquist, H. Högberg, J. M. Molina-Aldareguia, Zs. Czigány, Sz. Sasvári, P. O. Å. Persson, U. Jansson, and L. Hultman *Growth of Ti₃SiC₂ thin films by elemental target magnetron sputtering* Journal of Applied Physics 96 4817 (2004)
- ⁵ J. M. Molina-Aldareguia, J. Emmerlich, J.-P. Palmquist, U. Jansson, and L. Hultman *Kink formation around indents in laminated Ti₃SiC₂ thin films studied in the nanoscale* Scripta Materialia 49 155 (2003)
- ⁶ S. Zhang, D. Sun, Y. Fu, and H. Du *Toughening of hard nanostructural thin films: a critical review* Surface and Coatings Technology 198 2 (2005)
- ⁷ S. Zhang, D. Sun, Y. Fu, and H. Du *Toughness measurement of thin films: a critical review* Surface and Coatings Technology 198 74 (2005)

9 Additional results

“-Remember, son: Trying is just the first step towards failure.”

Homer Simpson

This chapter contains additional results from my PhD work; results that are relevant to the main topic of the Thesis but not included in the papers.

9.1 *In-situ* XPS of Ti-Si-C thin films

As discussed in section 7.2.1, X-ray Photoelectron Spectroscopy (XPS) is an important tool for surface analysis and composition determination. It further permits characterization of the different types of chemical bonds present in a material with very high surface sensitivity (a few nanometers). The issue of surface contaminants is often addressed by sputter-cleaning of the surface; a destructive process which may alter the composition and bonding configuration of the studied material. To avoid such effects, XPS can be performed *in situ*. Then, a sample is synthesized under ultrahigh-vacuum conditions, for example using sputtering. Through a transfer stage, the sample is then moved to the XPS analysis chamber without being exposed to atmosphere. This approach permits investigation of the pristine surface of the as-deposited film, without atmospheric contaminants and need for destructive cleaning processes.

Papers II and **III** show that there is excess C (compared to the target composition) in Ti-Si-C thin films deposited from a Ti_3SiC_2 target. As **Paper III** showed for films deposited at 300 °C, the C was primarily bonded to Ti and Si. The *ex-situ* XPS study in **Paper III**, however, could not provide information on the conditions of the pristine surface, since oxide formation and adsorption of hydrocarbides occur instantly upon exposure to atmosphere.

For *in-situ* XPS studies,^{*} Ti-Si-C thin films were deposited by magnetron sputtering from a Ti_3SiC_2 target[†] onto $\text{Al}_2\text{O}_3(0001)$ substrates. The target-to-substrate distance was in the range 60 – 125 mm. No substrate heating was applied. As-deposited films were transferred *in-situ* to the XPS analysis chamber.

^{*} I carried out the *in-situ* XPS experiments at the Center for Microanalysis of Materials, University of Illinois, which is partially supported by the U.S. Department of Energy under grant DEFG02-91-ER45439. I gratefully acknowledge Dr. Richard Haasch for invaluable assistance with *in-situ* XPS, and Prof. Ivan Petrov for the invitation and fruitful discussions.

[†] MAXTHAL® 312, courtesy of Kanthal AB

The *in-situ* XPS results showed that the Ti2p peak exhibited purely carbidic bonding (identical to the *ex-situ* XPS results in **Paper III**), and the Si2p peak position corresponded to predominant Si-C bonding. The C1s peak, on the other hand, exhibited an important difference to **Paper III**, in that two distinct peaks at 282.0 eV and 285.0 eV were found. These correspond to C-Ti and C-C bonding, respectively. Deconvolution revealed the presence of a weaker third peak at ~283.5 eV, corresponding to C-Si bonds. In comparison, the *ex-situ* XPS results (after sputter-cleaning) in **Paper III** showed that the C-Ti peak was dominant. In order to increase the surface sensitivity further, angle-resolved *in-situ* XPS measurement were performed on a set of Ti-Si-C thin films deposited at different target-to-substrate distance (60 mm – 125 mm at 4 mTorr Ar pressure) and pressure (4 – 24 mTorr at 100 mm target-to-substrate distance). Four different incidence angles were used: 90° (normal incidence) 60°, 30°, and 15°. The latter corresponds to an increase in surface sensitivity by a factor of ~5 compared to normal incidence. Figure 9.1 shows typical C1s spectra, from a film deposited for 20 min at 4 mTorr Ar pressure and a target-to-substrate distance of 125 mm. All spectra are normalized. It can be seen that the relative intensity of the C-C peak is higher for lower incidence angle; i.e., the C-C peak is surface-related. Thus, it can be concluded that there is a significant amount of free carbon present on the pristine surface of the Ti-Si-C film (i.e., before exposure to atmosphere).

Figure 9.2 shows X-ray photoelectron spectra from a film deposited under identical conditions as the film in Figure 9.1, but for 80 min; i.e., the deposition time was four times longer. Here, the surface-related C-C is even more dominant, indicating that C accumulates on the surface by continuous segregation during film deposition.

9.2 Mass spectrometry

Mass spectrometry is a useful tool for understanding sputtering processes. In particular, I am interested in sputtering from a compound target, the approach in **Papers II-V**. Mass spectrometry can provide information about what species are present and what their respective energy distributions are.

Figure 9.3 shows a schematic illustration of the setup used for energy-resolved mass spectrometry (PSM003, Hiden Analytical Inc.). The mass spectrometer consists of an energy filter (Bessel box) and quadrupole mass filter with electrostatic lenses in-between. The front was kept at floating potential and its orifice had a diameter of 300 μm . A secondary-electron multiplier detected positive ions. The mass spectrometer was mounted 14 cm from the target, in a 45° off-axis position. Note that the off-axis position of the mass spectrometer may adversely affect the measurement; however, on-axis mounting was not possible due to technical and geometrical constraints. The instrument was tuned with respect to Ar^{2+} ions. A Ti_3SiC_2 target[‡] with a diameter of 5 cm was sputtered in dc power-regulation mode with target powers at 25, 50, 100, 150 and 200 W with varying argon pressure of 2, 4, and 8 mTorr. Ion masses were scanned from 0.4 atomic mass units (amu) to 100 amu in steps of 0.2 amu, with the exception of the point 40.0 amu where no acquisition was performed, in order to avoid saturation by Ar^+ ions. In order to rule out any effect on the mass scans from differences between species in energy distribution, a set of verification mass scans

[‡] MAXTHAL® 312, courtesy of Kanthal AB

were performed at 200 W target power and 4 mTorr Ar pressure for five different energies (4, 8, 12, 16, and 20 eV). The energy distributions were measured from 0 to 10 eV for Ti and Si and from 0 to 20 eV for C.

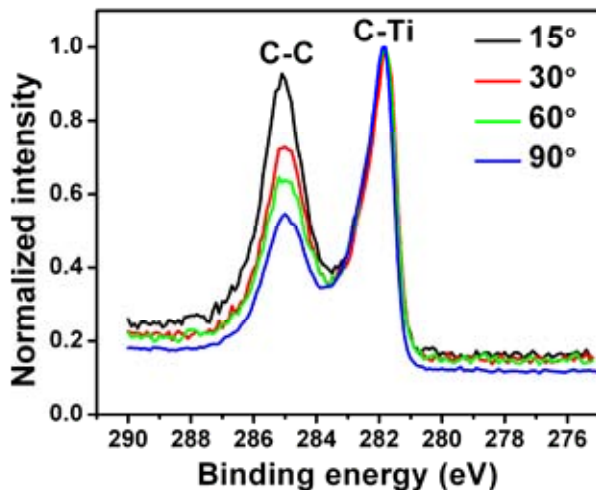


Figure 9.1 Angle-resolved *in-situ* X-ray photoelectron spectra of a Ti-Si-C thin film deposited for 20 min at room temperature from a Ti_3SiC_2 target.

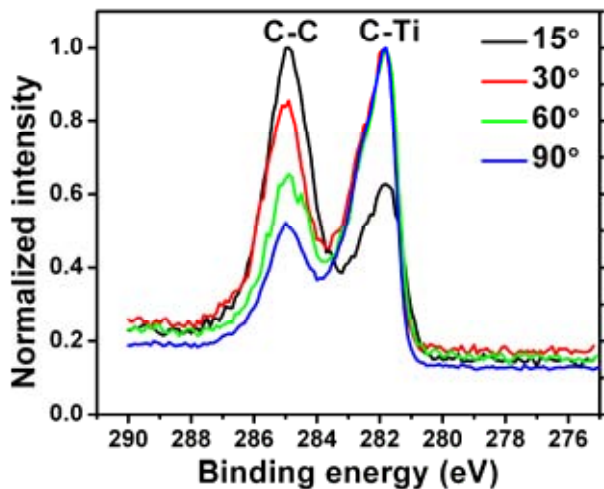


Figure 9.2 Angle-resolved *in-situ* X-ray photoelectron spectra of a Ti-Si-C thin film deposited for 80 min at room temperature from a Ti_3SiC_2 target.

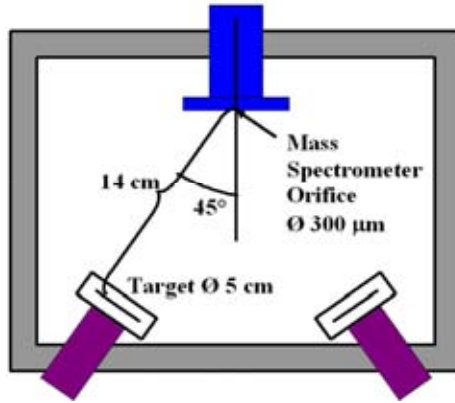


Figure 9.3 Schematic illustration of the setup for mass-spectrometry measurements to investigate the sputtering-deposition process.

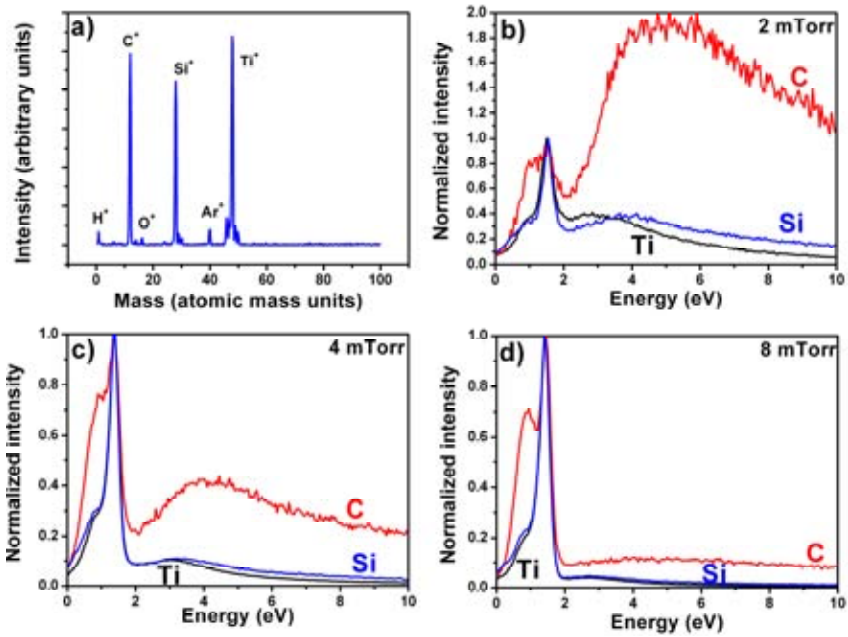


Figure 9.4 (a) Mass-scan of species in the sputtered flux from a Ti_3SiC_2 target operated at 200 W and 4 mTorr, and normalized energy distributions of Ti, Si, and C species at Ar pressures of (b) 2 mTorr, (c) 4 mTorr, and (d) 8 mTorr.

Figure 9.4(a) shows a typical mass scan performed at 200 W target power and 4 mTorr Ar pressure; mass scans performed at other parameters were essentially identical. Only Ti, Si, and C species can be seen, apart from H and O impurities originating from the residual gas, and Ar. No compound species, such as Ti-C, were detected. Additionally, Figure 9.4 shows normalized measured energy distributions of Ti, Si, and C for Ar pressures of 2 mTorr (Figure 9.4(b)), 4 mTorr (Figure 9.4(c)), and 8 mTorr (Figure 9.4(d)). It can be seen that, regardless of Ar pressure, the Ti and Si distributions exhibit a large peak at an energy of ~ 1.5 eV. This is the plasma potential, and corresponds to thermalized Ti and Si species. The energy distributions of C, on the other hand, are quite different. At Ar pressures of 2 – 4 mTorr, there is a large broad contribution to the energy distribution at higher energies (> 3 eV), corresponding to ballistic species. I.e., C is essentially not thermalized at 2 mTorr, and only to a limited extent at 4 mTorr.

These results are important to understand the sputtering process from a Ti_3SiC_2 target, as is a main objective of **Paper II** and to some extent also **Papers III – V**. Following the reasoning in **Paper II**, at an Ar pressure of 4 mTorr, the mean free path of C can be estimated to ~ 11 cm, while the corresponding mean free path of Ti and Si are much shorter, 2.5 and 5.8 cm, respectively. Correspondingly, at 4 mTorr, transport of C is predominantly in the ballistic regime, while Ti and Si are to a large extent thermalized. On the other hand, as seen in Figure 9.4(d), an Ar pressure of 8 mTorr resulted in suppression of the high-energy contribution to the energy distribution of C, i.e., a higher degree of thermalization than at low Ar pressure. The difference between species in distance to thermalization is an explanation for the high C content (see **Papers II and III**) in the film, in that Ti and Si species to a much larger extent than C suffer collisions (i.e., scattering) during transport from target to substrate. However, as shown in **Paper II**, the C content in the film remains much higher than the nominal 33 at. % C content also at the high Ar pressure of 16 mTorr, when all species are thermalized. Thus, gas-phase scattering cannot be the only explanation – the angular and energy distributions of species in the sputtered flux leaving the target must also be taken into account.[§]

[§] To be strict, the target geometry (i.e., the racetrack) and microstructure should also be considered.

10 Epilogue

*”-Now this is not the end.
It is not even the beginning of the end.
But it is, perhaps, the end of the beginning.”*

Winston Churchill

As I have now reached the end of the beginning – my Ph. D. studies – it may be worthwhile to stop and reflect on why I have done all this work. Was it for fun? Was it because I could work together with all these brilliant people? Was it for money? Was it because I could study fundamental physics and materials science, using a model system that is also interesting as a commercial product? Was it because I got to travel halfway around the world during my endeavors? The answer to all these questions is *Yes* – and I am sure there are many other reasons I did not think of right now.

But ultimately, it all condenses to what was so elegantly explained already in 1665, in the Introduction to the very first issue of the first scientific journal,^{*} the *Philosophical Transactions* (later *Philosophical Transactions of the Royal Society of London*):¹

Whereas there is nothing more necessary for promoting the improvement of Philosophical Matters, than the communicating to such, as apply their Studies and Endeavours that way, such things as are discovered or put in practise by others; it is therefore thought fit to employ the Press, as the most proper way to gratifie those, whose engagement in such Studies, and delight in the advancement of Learning and profitable Discoveries, doth entitle them to the knowledge of what this Kingdom, or other parts of the World, do, from time to time, afford, as well of the progress of the Studies, Labours, and attempts of the Curious and learned in things of this kind, as of their compleat Discoveries and performances: To the end, that such Productions being clearly and truly communicated, desires after solid and usefull knowledge may be further entertained, ingenious Endeavours and Undertakings cherished, and those, addicted to and conversant in such matters, may be invited and encouraged to search, try, and find out new things, impart their knowledge to one another, and contribute what they can to the Grand design of improving Natural knowledge, and perfecting all Philosophical Arts, and Sciences.

^{*} That is not strictly true: The first issue of the French *Journal des sçavans*, later *Journal des savants*, was published on January 5, 1665; the *Philosophical Transactions* appeared two months later, on March 6.

The introduction ends “*All for the Glory of God, the Honour and Advantage of these Kingdoms, and the Universal Good of Mankind.*”

I will let you, dear Reader, decide which of these reasons is more important to you. Personally, I would like to imagine that I have given my very small (nanoscale!) contribution to *the Universal Good of Mankind*. At the very least, the *Royal Society* were completely right in that nothing in science is more important than *communicating*, and I hope that you, dear Reader, have found my *Productions clearly and truly communicated*. That has been my intention from start to finish, and I humbly apologize in advance for any ambiguity, unclarity, or error you may find.

Finally, dear Reader, I *invite and encourage* you to pursue your own *ingenious Endeavours and Undertakings*, to *search, try, and find out new things*, *impart your knowledge to others*, and *contribute what you can to the Grand design of improving Natural knowledge, and perfecting all Philosophical Arts, and Sciences*.

I will make every effort to continue to do so, because I am *Curious*, and helplessly

addicted to such matters!

¹ *The Introduction* Philosophical Transactions 1 1 (1665) Accessible in digital format at the JSTOR database, www.jstor.org (March 10, 2007)